FEDERAL UNIVERSITY OF SÃO CARLOS
CENTER FOR EXACT SCIENCE AND TECHNOLOGY
GRADUATE PROGRAM IN MATERIALS SCIENCE AND ENGINEERING

REFILL FRICTION STIR SPOT WELDING OF DIFFERENT THICKNESS AL-CU ALLOY USING A TOOL WITH REDUCED DIMENSIONS FOR AEROSPACE APPLICATION

Murilo Feliciano de Lima Santos

São Carlos-SP
2020

FEDERAL UNIVERSITY OF SÃO CARLOS
CENTER FOR EXACT SCIENCE AND TECHNOLOGY
GRADUATE PROGRAM IN MATERIALS SCIENCE AND ENGINEERING

REFILL FRICTION STIR SPOT WELDING OF DIFFERENT THICKNESS AL-CU ALLOY USING A TOOL WITH REDUCED DIMENSIONS FOR AEROSPACE APPLICATION

Murilo Feliciano de Lima Santos

Masters Dissertation presented to Graduate Program in Materials Science and Engineering (PPGCEM) in partial fulfillment of the requirements for the MASTER OF SCIENCE DEGREE IN MATERIALS SCIENCE AND ENGINEERING

Supervisor: Dr. Nelson Guedes de Alcântara
Co-Supervisor: Dr. Athos Henrique Plaine
Funding Agency: CNPq - Process: 134356/2019-5

São Carlos-SP
2020

To our future generations, may they be better than we were

VITAE

Bachelor Degree in Materials Engineering from UFSCar (2019)

UNIVERSIDADE FEDERAL DE SÃO CARLOS

Centro de Ciências Exatas e de Tecnologia
Programa de Pós-Graduação em Ciência e Engenharia de Materiais

Folha de Aprovação

Defesa de Dissertação de Mestrado do candidato Murilo Feliciano de Lima Santos, realizada em 12/11/2020.

Comissão Julgadora:

Prof. Dr. Nelson Guedes de Alcântara (UFSCar)

Prof. Dr. Piter Gargarella (UFSCar)

Prof. Dr. Jorge Fernandez dos Santos (WMP/HZG)

O presente trabalho foi realizado com apoio da Coordenação de Aperfeiçoamento de Pessoal de Nível Superior - Brasil (CAPES) - Código de Financiamento 001.
O Relatório de Defesa assinado pelos membros da Comissão Julgadora encontra-se arquivado junto ao Programa de Pós-Graduação em Ciência e Engenharia de Materiais.

ACKNOWLEDGEMENTS

There are many people whom I should thank, not only for helping me with the conclusion of this project, but also for assisting me in becoming who I am today and steering me in the direction of who I want to become in the future.

I sincerely hope I have, at some point in time, let you all know how important you are to me. I also hope I can thank and repay each and every one of you frequently, for years to come. This should be worth more than I could ever scribble in a piece of paper.

Preferably, I would steer clear of naming names, because that would be doing a disservice to those I do not mention. However, I would be remiss not to mention my close family members Eduardo, Flávia and Carlos, and my friends Victória, Paulo, Dennis, Raphael, Pedro, Augusto, Lucas, Leonardo, Murilo, Nicoli, Natalia, Natascha, to name a few.

Furthermore, I would like to thank Professor Nelson G. Alcântara, Professor Athos H. Plaine and MSc Camila C. Castro for the technical guidance and productive discussions. I also want to thank Dr. Jorge F. dos Santos for the opportunity to work at HZG, an experience that has enriched me in many ways.

Finally, I would like to acknowledge the financial support by the CNPq (National Council for Scientific and Technological Development – Brazil – Process no. 134356/2019-5), CAPES (Coordination for the Improvement of Higher Education Personnel – Brazil), Helmholtz Association (Germany), in particular the Helmholtz Zentrum Geesthacht and the Shanghai Aerospace Equipment Manufacturer (SAEM - China). This study was financed in part by the Coordenação de Aperfeiçoamento de Pessoal de Nível Superior - Brasil (CAPES) - Finance Code 001.

ABSTRACT

Refill Friction Stir Spot Welding has grown as an interesting alternative to conventional joining techniques in recent years, especially when it comes to high strength aluminum alloys. Although current results show promise, there are still areas in which the body of knowledge is lacking and there are challenges for further investigation. This work tackled some of those challenges by investigating and optimizing the refill FSSW process for 2A12 (AA2024) aluminum alloy using a tool with reduced dimensions to weld an unconventional sheet configuration (0.8mm to 3mm in thickness). This was achieved using Design of Experiments coupled with Analysis of Variance. In addition, the influence of process parameters on microstructural geometrical features and in weld performance was studied, and Plunge Depth was found to be the most significant process variable when it comes to weld strength. Crack was shown to start around the hook region and propagate through two possible paths, the SZ/TMAZ interface or the aluminum rich layer in the stir zone. These two paths generated two main fracture modes, and the pullout mode was associated with the optimal condition. Given that a 2xxx series aluminum alloy was used, natural aging was investigated, and found to be influential in local mechanical properties through hardness tests. This influence, however, did not translate to Lap Shear Strength, as samples with different aging levels presented similar properties. Finally, the wear behavior of the tool was studied with increasing welding cycles. Tool geometry was significantly affected by wear, and this impacted weld surface with time, generating increasing notches on the edge of the stir zone. Those notches reduced the effective thickness of the top sheet, and consequently contributed to premature failure at inferior loads.

Keywords: Solid State Welding; Refill FSSW; 2A12; Design of Experiments; ANOVA; natural aging; tool wear.

RESUMO

SOLDAGEM A PONTO POR FRICÇÃO DE LIGA DE AL-CU DE DIFERENTES ESPESSURAS UTILIZANDO FERRAMENTA COM DIMENSÕES REDUZIDAS PARA APLICAÇÃO AEROESPACIAL

A soldagem por fricção por ponto (Refill FSSW) tem se mostrado uma alternativa interessante para substituir métodos de soldagem convencionais nos últimos anos, especialmente em se tratando de ligas de alumínio. Apesar de as pesquisas serem promissoras, ainda há muitas áreas inexploradas no tema. O presente projeto visou avaliar algumas dessas áreas através da investigação e otimização do processo de Refill FSSW para a liga de alumínio 2A12 (AA2024) usando uma ferramenta de dimensões reduzidas para soldar uma configuração de chapas não convencional (0,8mm com 3,0mm). Isso foi realizado através da utilização de Planejamento Estatístico de Experimentos e Análise de Variância. Adicionalmente, a influência dos parâmetros do processo em características microestruturais geométricas e na performance das soldas foi estudada, e a profundidade de penetração apresentou-se como a variável mais significante no que diz respeito à resistência mecânica das soldas. Observou-se que trincas se iniciam no *hook* e se propagam através de dois possíveis caminhos, a interface entre SZ e TMAZ ou a camada rica em alumínio no centro da solda. Esses dois caminhos possíveis resultam em dois modos de fratura. O envelhecimento natural foi investigado, e apontado como influente em propriedades mecânicas locais através de ensaios de dureza. Essa influência, contudo, não se traduziu para a resistência ao cisalhamento, uma vez que amostras em diferentes estágios do envelhecimento apresentaram propriedades similares. Por fim o comportamento de desgaste da ferramenta foi estudado com o aumento dos ciclos de soldagem. A geometria da ferramenta foi significativamente afetada pelo desgaste, e impactou na superfície das soldas, gerando indentações na borda externa da zona de mistura. Essas indentações reduziram a espessura efetiva das chapas e contribuíram para a falha precoce em cargas inferiores.

Palavras-chave: Soldagem no estado sólido; Refill FSSW; 2A12; Planejamento de Experimentos; ANOVA; envelhecimento natural; desgaste de ferramenta.

TABLE OF CONTENTS

Pág.

LIST OF TABLES

LIST OF FIGURES

SYMBOLS AND ABBREVIATIONS

AA	Aluminum Association
ANOVA	Analysis of Variance
ASTM	American Standard for Testing of Materials
AWS	American Welding Society
BBD	Box-Behnken Design
BM	Base Material
CCD	Central Composite Design
CCDM	Center for Materials Development and Characterization
CNPq	Scientific and Technological Development National Council
DoE	Design of Experiments
DSC	Differential Scanning Calorimetry
FFD	Full Factorial Design
FSpW	Friction Spot Welding
FSSW	Friction Stir Spot Welding
FSW	Friction Stir Welding
GKSS	Gesellschaft für Kernenergieverwertung in Schiffbau und Schiffahrt
HAZ	Heat Affected Zone
HZG	Helmholtz Zentrum Geesthacht
LSS	Lap Shear Strength
LSW	Laser Spot Welding
OFAT	One-Factor-At-a-Time
Refill FSSW	Refill Friction Stir Spot Welding
RSM	Response Surface Methodology
RSW	Resistance Spot Welding
SEM	Scanning Electron Microscope
SFJ	Spot Friction Joining
SZ	Stir Zone
TMAZ	Thermomechanically Affected Zone

1 INTRODUCTION

For the past few decades, humanity strode towards lightweight solutions in many industrial applications, which led to a significant increase in research and development investment in this field. Among the industries that helped lead the charge in investigating these solutions was the transportation industry, which is always focusing on increasing cost-effectiveness and energy efficiency.

One of the main challenges faced when working with lightweight materials is related to their joining processes. Some aluminum alloys, in particular, cannot be properly welded by conventional welding techniques. Fusion-based processes such as Resistance Spot Welding (RSW) and Laser Spot Welding (LSW) require great energy input due to the metal's high electrical and thermal conductivities, incurring high operational costs. Additionally, oxide/hydroxide layers, dissolved hydrogen, and other solidification problems are well-known drawbacks from these processes [1–3]. Alternatively, mechanical fastening techniques, such as riveting, are widely applied to join lightweight materials. However, aside from the obvious weight penalty imposed by adding the rivet, there are disadvantages associated with low corrosion resistance, high cost of drilling, difficulty of automation, low efficiency, and a requirement for sealants [1, 2, 4–6]. Dissimilar materials may also pose a welding challenge due to undesired intermetallic compound formation during the solidification process [7–9].

In this context, solid-state joining processes, especially friction-based, have emerged in recent years as an attempt to mitigate those issues and have been showing promising results ever since. The most recent development in spot joining is Refill Friction Stir Spot Welding (Refill FSSW) also known as Friction Spot Welding (FSpW). This technique has been successfully used to join several similar and dissimilar combinations.

Even though current results show promise, there is still a lot to explore in the field, given that only very specific tool dimensions and sheet configurations have been studied so far. In order to shrink some of these knowledge gaps, this work aimed to analyze previously researched Al-Cu alloys for aerospace applications using novel sheet dimensions: 0.8mm top sheet and 3.0mm bottom sheet. The former is thinner, and the latter is thicker than the typically used

sheets. Additionally, the study was performed using a toolset with 5-mm adjustable shoulder and 3.3-mm probe. These dimensions are considerably smaller than the typical Refill FSSW tool, which allowed for an investigation of the technical feasibility of using this method to join smaller areas, as well as comparison with other joining methods.

To achieve this, optimization methods were utilized to obtain welds with high mechanical performance, as well as to understand how process variables influence Lap Shear Strength and microstructural features. Subsequently, mechanical testing and cross-section observation were used to investigate the different types of failure. Additionally, thermal cycle measurements, and mechanical testing were used to evaluate how post-welding natural aging occurs. Finally, the wear behavior of the tool was investigated and its impact on mechanical performance was measured. Compiling those investigations, a comprehensive view of the process was obtained, assisting with the technological development of Refill FSSW.

2 OBJECTIVES

The main objective of this study was to perform a technical feasibility analysis and optimize the Refill Friction Stir Spot Welding process in 2A12-T6 sheets of different thicknesses (namely 0.8mm to 3.0mm), to be used in aerospace applications, using a tool with reduced dimensions.

Specifically, this study aims to:

- Apply Design of Experiments (DoE) through Box-Behnken Design and Analysis of Variance (ANOVA) to optimize the mechanical properties of the joint, as well as to comprehend the process parameter's influence on weld performance.
- Understand microstructure-processing relationships that govern the Refill FSSW process in this specific welding configuration, and how it might affect properties.
- Evaluate the mechanical behavior of the welds through lap shear tests and failure mechanism observation. Understand crack origin and preferable propagation paths through loading-unloading experiments, identifying the weakest points in the weld.
- Investigate metallurgical aspects consequential to the welding process through thermal cycle observation, natural aging investigation, and measurement of its impact on global and local mechanical properties.
- Understand how tool wear progresses with increasing number of welding cycles. Investigate possible impacts on weld surface and on Lap Shear Strength and propose a preliminary mechanism for the observed behavior.

3 LITERATURE REVIEW

3.1 Aluminum alloys

3.1.1 Aluminum alloys in aerospace applications

Aluminum and its alloys have been a viable engineering option since the end of the 1800s mainly because of its light weight. As previously stated, in recent human history, lighter structures became a big ambition of the industrial and scientific communities, especially the transportation industry. Lightweight is key to this sector because it leads to making a structure deliver the same or even enhanced performance with less material. This ultimately generates increased speed or payload capacity, cheaper structures, less fuel consumption, and thus less greenhouse gas emissions, the last one being of higher importance with every year that goes by [10, 11]. Since it has been shown that decreasing density is one of the most effective ways to decrease overall aircraft weight, being 3 to 5 times more effective than increasing tensile strength, elastic modulus, or damage tolerance [12], materials with this characteristic have been a preferable choice for manufacturers.

Among the efforts to find lightweight materials, several companies and research studies found aluminum alloys to be promising solutions for several applications in the automotive and aerospace sectors. Aluminum is a recyclable material that aside from low density, has high specific properties, good corrosion behavior, high thermal and electrical conductivities and low cost. The material's most interesting feature, however, is versatility. With more than three hundred listed alloy compositions and numerous heat and thermo-mechanical treatments, a wide range of physical and mechanical properties can be obtained with this material [13, 14].

Even though this has been noted experimentally for more than a hundred years in the aerospace sector, and the research was well-established long ago [15, 16], it is evident that aluminum alloys still have an important role in these applications. This happens not only because of their well-known performance but also for their reliable inspection methods, established processing routes, and deep metallurgy understanding [12]. This enables this group of materials to

compete with the rapid-rising composites and hybrid structures, and hold a significant share of the market in the applications mentioned [10, 12, 16, 17]. This is observable in the material distribution of a few Boeing products, presented in Figure 1 [10].

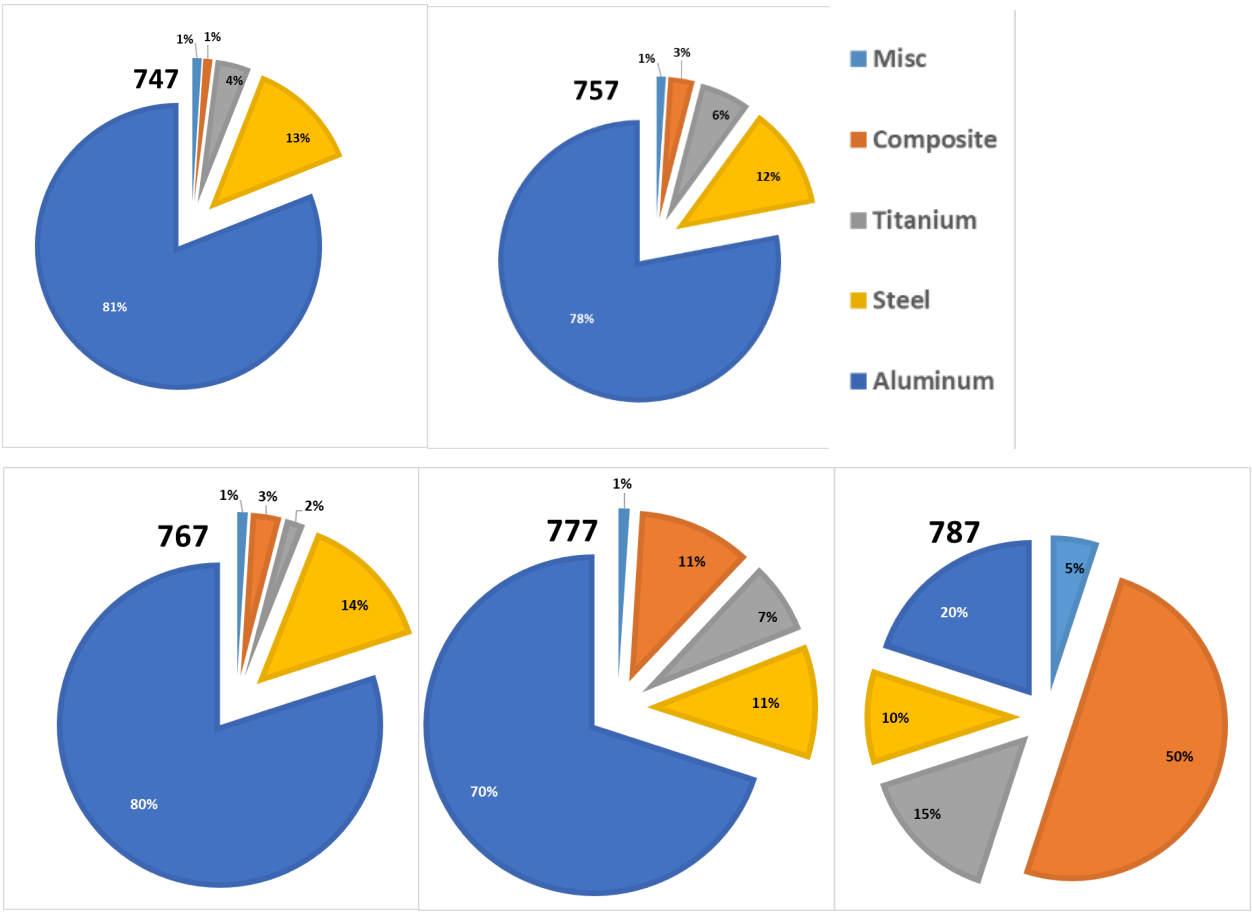

Figure 1 - Material distribution for Boeing products [10].

3.1.2 AA2024-T6 alloy

The AA2024 alloy is part of the 2xxx series of aluminum alloys, which is a heat-treatable series of alloys. These alloys suffer precipitation and strengthening and are often called age-hardening alloys. Precipitation hardening was discovered in 1906 [18] and was studied throughout the years, with diverse theories to explain nucleation and growth of phases being proposed [14]. Wang and Starnik [19, 20] have done extensive research and a comprehensive review of precipitation in 2xxx series alloys.

With copper as the main alloying element, the first heat treatable alloy discovered was from the 2xxx series [14] and the Al-Cu system quickly became the most studied system to understand age hardening. It is considered one of the most complex systems among this type of alloys [18].

In the Al-Cu system, precipitation follows the order:

Supersaturated Solid Solution → GP Zones → θ'' → θ' → θ

Magnesium is frequently added to the Al-Cu alloys and enhances both rate and magnitude of natural aging [14]. It also decreases the density of the alloy while increasing its strength [18]. These magnesium-enriched alloys can be divided into four phase fields, as seen in Figure 2. The main field for industrial applications is the α+S field, in which precipitation happens as follows:

Supersaturated Solid Solution → Cu-clusters → GPB Zones → S' → S

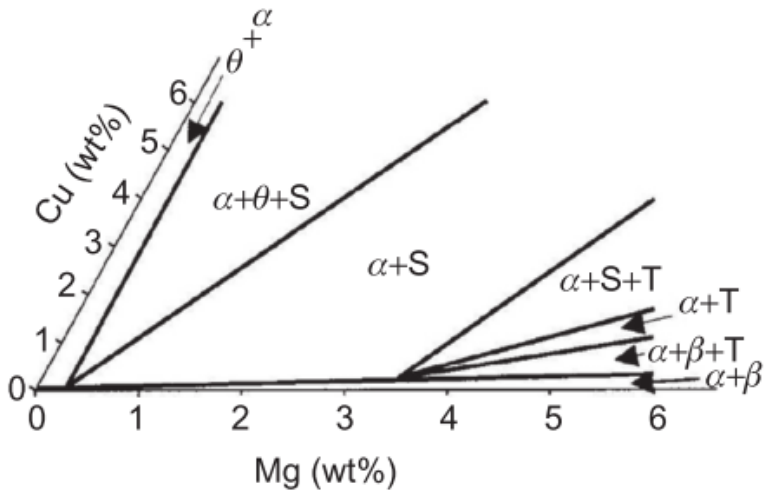

Figure 2 - Isothermal section of the ternary Al-Cu-Mg diagram at 200ºC [19].

In the 2xxx series, a significant amount of hardening takes place at room temperature. This is called the natural aging process. Thus, several alloys are used in the T3 and T4 tempers. Usually, most of the hardening happens in the first 24 hours, and stability is reached after four days [14].

3.2 Refill Friction Stir Spot Welding

3.2.1 Process Stages, Equipment, and State of the Art

Friction-based joining processes were developed aiming to mitigate the previously mentioned metallurgical issues associated with the welding of lightweight materials. In spot-like configuration, two important processes based on Friction Stir Welding were simultaneously established [21]. Kawasaki introduced the Spot Friction Joining (SFJ) technique, now known as Friction Stir Spot Welding (FSSW), and described in US patent 6,601,751 B2 [22]. In the meantime, Helmholtz-Zentrum Geesthacht (formerly known as GKSS) developed Refill Friction Stir Spot Welding (Refill FSSW), sometimes referred to as Friction Spot Welding (FSpW). The process is described in US patent 6,722,556 B2 [23].

The Refill FSSW process uses a three-piece tool consisting of a clamping ring, adjustable shoulder, and probe, all concentric, and assembled as shown in Figure 3. While the outermost part (clamping ring) is stationary, adjustable shoulder and probe are rotatable parts moved by the same motor. All parts have axial movement controlled by separate actuators, allowing them to be independently vertically displaced.

Figure 3 - Refill Friction Stir Spot Welding tool pieces and assembly.

The process can be divided into four steps, depicted in Figure 4. Once it starts, the whole tool advances and the clamping ring applies pressure on the overlapping to-be-welded sheets against a backing anvil, while both shoulder and probe start to rotate (a). Then, the shoulder plunges into the top sheet, plasticizing the material by frictional heat while the probe retracts in a volumetrically equivalent manner (b). Subsequently, a refilling stage takes place (hence, the

name of the technique) in which adjustable shoulder and probe return to their original positions. At this point, the plasticized material is pushed by the probe into the cavity left by the retracting shoulder (c). Finally, the tool is lifted (d) leaving a flat surface without a keyhole, characteristic of processes such as FSW and FSSW [2, 24]. This variant of the process is called shoulder-plunge variant, once the adjustable shoulder is the plunging element, as opposed to the probe-plunge variant, in which the probe plunges first into the top sheet, while shoulder retracts in stage (b). The former of the processes is the one utilized in this study and has been more widely researched, mostly due to its larger resulting welded area [2, 5].

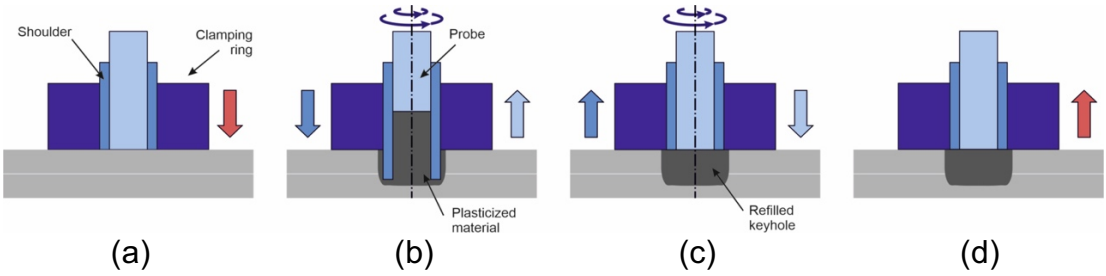

Figure 4 - Refill Friction Stir Spot Welding process, schematically illustrated in steps.

Among those efforts already made to enhance understanding of Refill Friction Stir Spot Welding diverse combinations of materials were studied with different approaches and focuses. A handful of authors studied 2xxx series aluminum alloys in similar configuration [1, 2, 4, 6, 25–29], a few more have studied other alloys such as AA6181 [30], AA5042 [21], AA6061 [31], AA7075 [32, 33], AA7050 [34, 35], Al-Mg-Si [36] and Al-Mg-Sc [37]. Aluminum has also been investigated in dissimilar configurations, coupled with magnesium [3, 8, 38, 39], copper [7, 40], steel [3], and Titanium [9, 41, 42]. Magnesium alloy AZ31 was studied in similar configuration [5]. Refill Friction Stir Spot Welding has also been used to join thermoplastics with aluminum [43, 44].

These studies have had a wide variety of purposes, investigating process optimization, influence of parameters on microstructure and properties of the weld [1, 2, 30, 33, 34, 36, 41, 43, 3–6, 21, 25, 27, 29], defect formation, failure modes, intermetallic formation [7–9], thermal cycle [38], fatigue life [26, 35, 42],

flow behavior [37], corrosion behavior [45] and usage as a keyhole closure method [28, 31, 32]. A summary of these studies can be found in Table 1.

Table 1 - Summary of references containing authors, material combination, and main focus of study.

Reference Index	Authors	Material Combination	Main Focus
1	Da Silva et al.	AA2024 - T3	Optimization and Parameter Influence
2	Tier et al.	AA2024 - T3	Optimization and Parameter Influence
3	Suhuddin et al.	Multiple combinations*	Optimization and Parameter Influence
4	Amancio et al;	AA2024 - T3	Optimization and Parameter Influence
5	Campanelli et al.	AZ31	Optimization and Parameter Influence
6	Li et al.	AA2024	Optimization and Parameter Influence
7	Shen et al.	AA5083/Cu	Eutetic Structure Formation
8	Suhuddin et al.	AA5754/AZ31	Intermetallic Formation
9	Plaine et al.	AA5754/Ti-6Al-4V	Defect Formation, Failure modes and Intermetallic formation
21	Tier et al.	AA5042	Optimization and Parameter Influence
25	Pieta et al.	AA2198-T8	Optimization and Parameter Influence
26	Brzostek et al.	AA2024-T3	Fatigue Life
27	De Barros et al.	AA2198-T8	Optimization and Parameter Influence
28	Reimann et al.	AA2198-T851	Keyhole Closure Method
29	Ji et al.	AA2024-T4	Optimization and Parameter Influence
30	Rosendo et al.	AA6181-T4	Optimization and Parameter Influence
31	Reimann et al.	AA6061-T6	Keyhole Closure Method
32	Reimann et al.	AA7075-T651	Keyhole Closure Method
33	Kubit et al.	AA7075-T6	Optimization and Parameter Influence
34	Effertz et al.	AA7050-T76	Optimization and Parameter Influence
35	Effertz et al.	AA7050-T76	Fatigue Life
36	Santana et al.	Al-Mg-Si	Optimization and Parameter Influence
37	Shen et al.	AlMgSc	Material flow
38	Suhuddin et al.	AA5754/AZ31	Thermal Cycle
39	Suhuddin et al.	AA5754/AZ31	Optimization and Parameter Influence

40	Shen et al.	AA5083/Cu	Optimization and Parameter Influence
41	Plaine et al.	AA6181-T4/Ti-6Al-4V	Optimization and Parameter Influence
42	Plaine et al.	AA5754/Ti-6Al-4V	Fatigue Life
43	André et al.	AA2024-T3/CF-PPS	Optimization and Parameter Influence
44	André et al.	AA2024-T3/CF-PPS	Interlayer Film influence on Properties
45	Vacchi et al	AA6181-T4/Ti-6Al-4V	Corrosion behavior

*This is a review paper on multiple combinations containing the following alloys: AA6181-T4, AZ31, DP600

Among the studies presented in Table 1, most show the optimized strength of the welds far surpassing the minimum requirement for Resistance Spot Welding imposed by the AWS D17.2/D17.2M:2013 standard for aerospace applications [46]. It is important to point out, however, that throughout these studies there is no uniformity in the optimal parameters, meaning that modifying the material used, the tool dimensions or the sheet configuration requires a new optimization process.

3.2.2 Microstructure in Refill FSSW

A typical Refill Friction Stir Spot Welding microstructure is displayed in Figure 5. In the central region of the weld is the Stir Zone, indicated by “SZ”. In this region, both the process temperatures and the shear rates originated by tool rotation are at a maximum. This generally leads to dynamic recrystallization in the area and generates a distribution of fine and equiaxed grains. Adjacent to this region is the Thermomechanically Affected Zone (TMAZ), where moderate shear rates and temperatures usually promote partial recrystallization which yields slightly elongated grains, rotated about 45^{o}.

Outside the TMAZ, the Heat Affected Zone (HAZ) remains unaffected by plastic deformation, being subject only to transformations from the thermal cycle experienced by the process. Thus, the HAZ can have slightly larger grains and diminished local mechanical properties due to precipitate overaging (in age hardening alloys). As the distance from the

center of the weld increases, experienced temperatures decrease, up to a point where they do not have any influence on the material. From this point onwards, characteristics of the Base Material (BM) are observed.

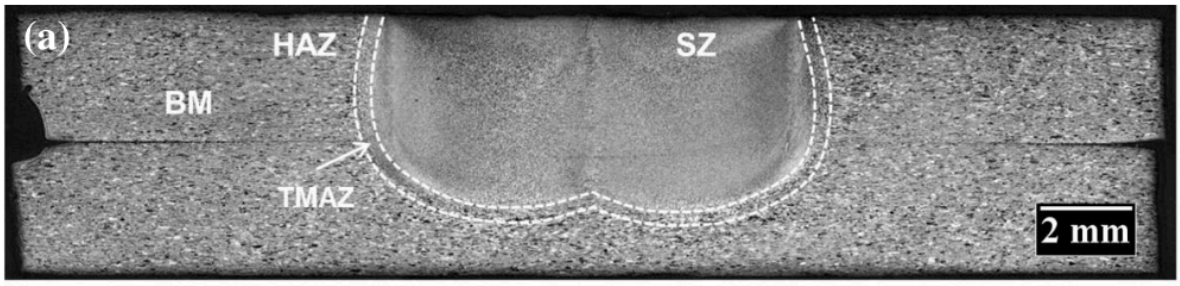

Figure 5 - Typical RFSSW microstructure [36].

Aside from these well-known microstructural regions, a few other features have been described. Several authors report especially the presence of defects such as lack of mixing, incomplete refill, voids, partial bonding, and hooking [5, 30, 36].

3.2.3 Failure Types in Refill FSSW

When it comes to failure in RFSSW under static loading, several naming standards and variations can be found in the literature for different failure types [5, 6, 27, 34]. The two most established major identifications for these types are “pullout” and “through the weld”. In the pullout mode, crack propagates around the weld nugget, which stays attached to the bottom sheet as the top sheet detaches. In the through the weld mode, on the other hand, crack propagates parallel to the original interface between sheets, going through the stir zone and shearing this interface.

In Alclad AA2024, Li et al. [6] identified four types of failure and discussed how the bonding, heat input, microstructure and hardness aspects interact to cause the different failure types. Campanelli et al. [5] performed similar work in the magnesium alloy AZ31, analyzing fracture surfaces and strongly correlating hook height to different failure types.

3.2.4 Refill FSSW Tool Wear

One aspect of friction-based processes which remains slim in terms of research is tool wear, with very few papers published, especially in Refill FSSW. This aspect, however, is extremely important to guarantee reproducibility and homogeneity of the welds, which in turn are paramount to large scale industrial applications.

Shen et al. [47] investigated the impact of tool design in weld quality and strength by comparing a standard tool design to a modified tool design with grooves and notches. This adapted tool geometry was shown to be associated with better bonding, resulting in defect-free welds as opposed to the defective welds produced with the standard tool.

Nasiri et al. [48] performed an extensive failure analysis after extremely premature failure was observed in the welding of Al-2099 alloy after four to six welds. In this study, high lithium content and the temperatures experienced led to second phase formation, and subsequent melting, inside the gap between tool parts. This promoted interaction between the liquid phase and the tool steel, generating a liquid metal embrittlement effect.

Montag et al. [49] investigated the progressive wear on Refill FSSW tools through 3500 welding cycles of 2 mm AA6082-T6 sheets and proposed a mechanism to explain its occurrence. Even though the Lap Shear Strength of the welds were not affected by the wear in this particular case, the authors raised a concern on the economic aspects of having correct tool replacement time.

De Castro [50] performed a comprehensive study on the evolution of tool wear and its impact on weld strength and microstructural features by welding AA2198-T8 sheets. The author showed a decreasing trend in strength and microhardness along 2350 welding cycles, promoted by two distinct mechanisms of wear. A causal relation between wear, tool dimension reduction, stir zone area reduction, and strength reduction was established.

When analyzing this body of work, it is evident that the research surrounding the wear behavior of Refill FSSW tools is indeed incipient. Furthermore, a wide range of tool lifecycles can be observed between the

different studies, which indicates that the behavior of tool wear has high variability and needs to be further investigated, in order to guarantee correct tool usage.

3.3 Design of Experiments

Diverse industrial sectors usually need to experiment while developing a new product, optimizing processes, or looking to improve the overall quality of a given output. For this to happen, experimentation is necessary. Humanity has dealt with experimentation for a long time, and diverse systematic approaches to conducting experiments have been proposed since Sir Ronald Fisher's work in agriculture in the 1920s [51, 52].

A well-designed experiment is extremely important, for the results and conclusions drawn from it depend to a large extent on how the experiments were performed [53]. Therefore, relying on proven statistical methods to analyze experiments became a trend for scientific research. The basic statistical principles for a designed experiment are replication, randomization, and blocking [51]. The assembly of these statistical tools and methods is commonly referred to as Design of Experiments (DoE) and is often used effectively to plan, design, and analyze experiments to draw conclusions.

One of the simplest yet effective methods of experimentation is the one-factor-at-a-time (OFAT) approach. This technique consists of choosing a set of factors to vary and initial values for each one of them, then varying one factor through its range while keeping the others constant. After doing that successively for each factor, the experimenter analyses the outputs. One major drawback is that this method fails to evaluate possible interactions between factors [53].

A good way of drawing conclusions from a certain process while accounting for its interactions is to perform experiments in every possible combination of factors. This process is called a full factorial design (FFD). Despite being useful, when the number of factors or levels increase, the amount of runs necessary for the experiment grows impossible to perform [53].

Another popular approach to designed experiments developed in the 1980s is the Taguchi method. This method was created based on a quality philosophy that aims to achieve optimized results by minimizing the deviation

from a target value and among different observations [52]. This method is powerful in its experimental efficiency. For example, a full-factorial design with 15 factors at two levels would require 32,768 (2^{15}) test runs, while by the Orthogonal Array of the Taguchi methodology it is possible to fit this experiment in 16 runs. However, the more complex the interactions between factors, the less accurate is the model. To properly account for interactions, one must know which interactions to observe in advance and include them in the orthogonal array using linear graphs [52].

Response Surface Methodology (RSM) is a collection of statistical and mathematical tools to use regression models to fit the response of interest (y) as a function of the process parameters, treated as variables ($x_1, x_2, \dots, x_n$), and the error (ϵ):

$$y = f(x_1, x_2, \dots, x_n) + \epsilon$$

It is a useful technique when optimization and analysis of parameter influence are required [53]. One of the possible methods to apply RSM is the Box-Behnken Design, which is going to be further detailed in the following section.

3.3.1 The Box-Behnken Design

In 1960, Box and Behnken proposed an incomplete three-level design to fit response surfaces. This design, referred to as Box-Behnken, consists of a particular combination of 2^k factorial with incomplete block design [51, 53].

When used with three factors, it consists of performing a full factorial 2^2 experiment with the third factor kept constant at an intermediate level plus a chosen number of center points (in which all factors are at their mean level). Thus, the variables of interest are coded into (-1) for their lower levels, (+1) for the higher levels and (0) for the mean levels. This generates the experimental runs shown in Table 2.

Table 2 - Coded factor levels for a Box-Behnken design in a three-variable system [54].

Experimental Run	x_1	x_2	x_3
1	-1	-1	0
2	1	-1	0
3	-1	1	0
4	1	1	0
5	-1	0	-1
6	1	0	-1
7	-1	0	1
8	1	0	1
9	0	-1	-1
10	0	1	-1
11	0	-1	1
12	0	1	1
Center (C_0)	0	0	0

Figure 6 graphically represents these incomplete blocks of full factorial designs. To aid in visualization, these runs can also be fitted in a cube with experimental points on the middle of its edges, as shown in Figure 7.

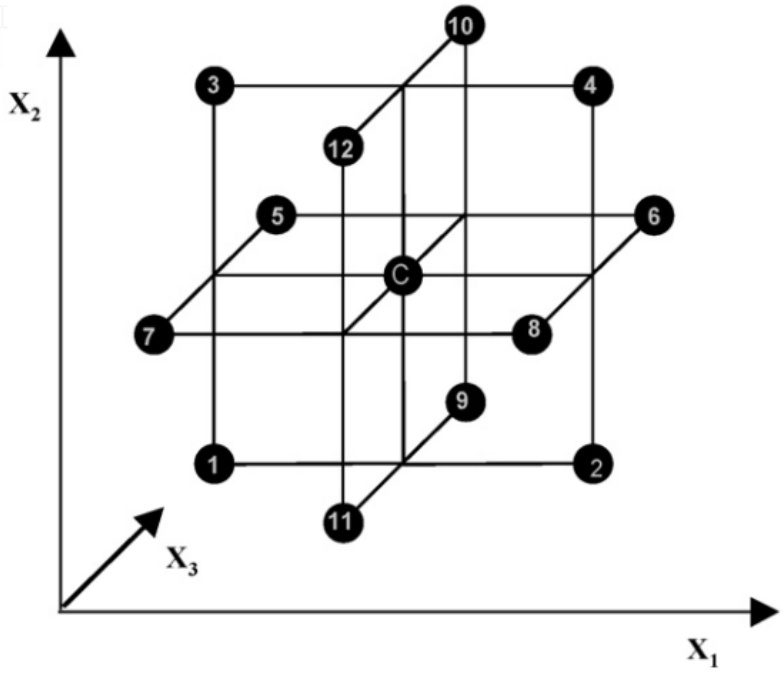

Figure 6 - Graphical representation of the three interlocking blocks of 22 of a three-variable Box-Behnken Design [54].

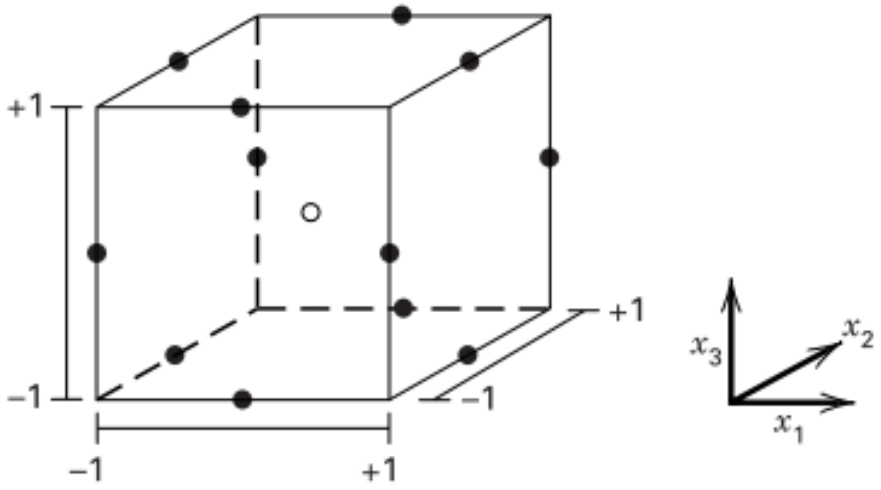

Figure 7 - Graphical representation of a three-variable Box-Behnken Design cube [53].

This configuration grants rotatability to the design, once the measured points are equidistant from the design center. In a rotatable design, the variation of the predicted response is constant with the distance for the center of the design (i.e. the variance is constant on spheres centered at the center point of the design). This ultimately means that the model is not biased in any direction of prediction, and thus makes the property a reasonable basis for the selection of the Response Surface Design [53].

The center points are performed to provide a reasonable estimation of the variance of the predicted response. Usually, three or five runs are performed [53]. Therefore, the final number of experiments required for this design with k factors and C_0 center points is $N = 2k(k-1) + C_0$ [54].

This makes Box-Behnken slightly more efficient than other designs to fit response surfaces such as Central Composite Design and much more efficient than Full-Factorial Designs, as shown by Ferreira et al [54]. Aside from the number of required runs, another reason for choosing Box-Behnken instead of CCD for this particular project is that Face-Centered CCD is not rotatable, whereas CCD's rotatable versions, Inscribed CCD (CCI) and Circumscribed CCD (CCC), have a smaller volume of analysis and prohibitive axial points, respectively [51, 53].

Results obtained using this methodology can be submitted to analysis of variance (ANOVA) to assess the influence of the factors in the response. All these features make Box-Behnken an interesting tool, being applied successfully in diverse fields of science to design experiments [55–57], including Refill FSSW [36].

3.3.2 Analysis of Variance (ANOVA)

One effective tool widely used to analyze data from a factorial experiment is the analysis of variance (ANOVA). Initially used to identify differences between treatments (i.e. levels of a single factor) in the One-Way ANOVA, this analysis can be extrapolated to analyze factorial experiments as Multi-Way ANOVA.

The ANOVA name derives from partitioning the variability into its component parts. The technique uses sums of squares as a measure of the overall variability in the data. This allows investigation between and within treatments to be performed [53]. For two factors, for example, the fixed effects model is described by:

$$y_{ijk} = \mu + \tau_i + \beta_j + (\tau\beta)_{ij} + \epsilon_{ijk} \quad \begin{cases} i = 1,2,\dots,a \\ j = 1,2,\dots,b \\ k = 1,2,\dots,n \end{cases}$$

Where μ is the overall mean effect, τ_i is the effect of the ith level of the row factor A, β_j is the effect of the jth level of column factor B, $(\tau\beta)_{ij}$ is the effect of the interaction between τ_i and β_j, and ϵ_{ijk} is a random error component. When this model is used, the difference between treatments and the significance of interaction between them is measured using several null hypotheses, and the F-test of a statistic thoroughly described by Montgomery et al. [53].

4 MATERIALS AND METHODS

4.1 Work Plan

Aiming to fulfill the objectives proposed, the work was divided into a few stages, which will be presented and clarified in this section. Initially, the manufacturing of the welds took place during the author's internship in the Helmholtz Zentrum Geesthacht (HZG), in 2018. At that same period, data originated from the thermal monitoring of the process and the Lap Shear Strength of the welds were also collected.

The processing and interpretation of said data was carried out during the master's degree period. This was the foundation for the statistical optimization of the process and evaluation of the process parameter's influence on welding features. Subsequently, the work was split into three main fronts: mechanical and metallurgical investigations and tool wear analysis.

In the mechanical portion of the work, the failure mechanisms were categorized and evaluated through optical microscopy. Afterwards, loading-unloading experiments were performed to understand crack initiation sites and preferable propagation paths.

The metallurgical effects of the process were evaluated primarily through the observation of the thermal cycle of the process. The impact of the Natural Aging effect was measured through local (microhardness) and global (Lap Shear Strength) mechanical properties.

Additionally, a tool wear investigation was carried out. The effect of successive welding on tool geometry was analyzed in a digital and a confocal laser microscope. Subsequently, the effect of this deformation on weld surface and mechanical properties was analyzed.

A schematic representation of the workflow described is depicted in Figure 8. The materials and specific methods used are presented in the following section.

Figure 8 - Proposed workflow and project progress.

4.2 Materials

The materials used for welding were provided by the Shanghai Aerospace Equipment Manufacturer, with nominal chemical composition listed in Table 3. The 2A12 alloy is chemically equivalent to the AA2024 alloy [13], however, due to geographical supply, the sheets were received according to Chinese standards. The material was received in the form of sheets with dimensions shown in Figure 9, after receiving a coating of 99% pure aluminum (commercially known as Alclad).

Table 3 - Nominal composition of the received alloys.

Alloy	**Composition, weight%**									
	Si	Fe	Cu	Mn	Mg	Cr	Zn	Ti	Others	Al
2A12	0.5	0.5	3.8-4.9	0.3-0.9	1.2-1.8	0.1	0.25	0.15	0.05-0.15	Bal.

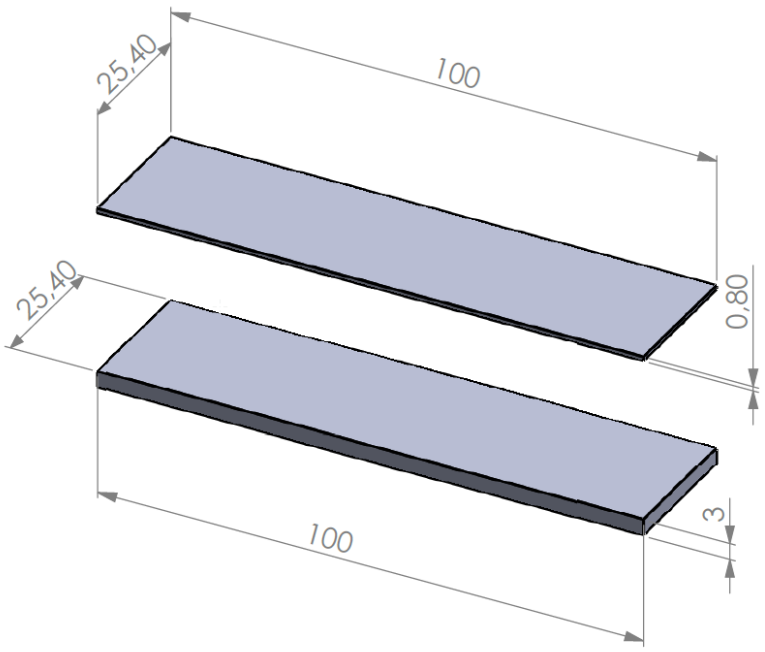

Figure 9 - Sheets received, dimensions in mm.

4.3 Methods

4.3.1 Welding & Design of Experiments

All welds were carried out in a Harms & Wende RPS 100 V32® machine. This machine possesses a C-Frame, which makes it a more suitable choice for industry-translatable research, unlike the previous RPS100 model.

Aiming to replace smaller rivets, the chosen tool design has dimensions significantly smaller than the most widely used tools. Clamping ring, adjustable shoulder, and probe have 17mm, 5mm, and 3.3mm diameter respectively, as opposed to 17mm, 9mm, and 6mm in the typically used, conventional tools. A schematic of a partially overlapped weld sample is shown in Figure 10.

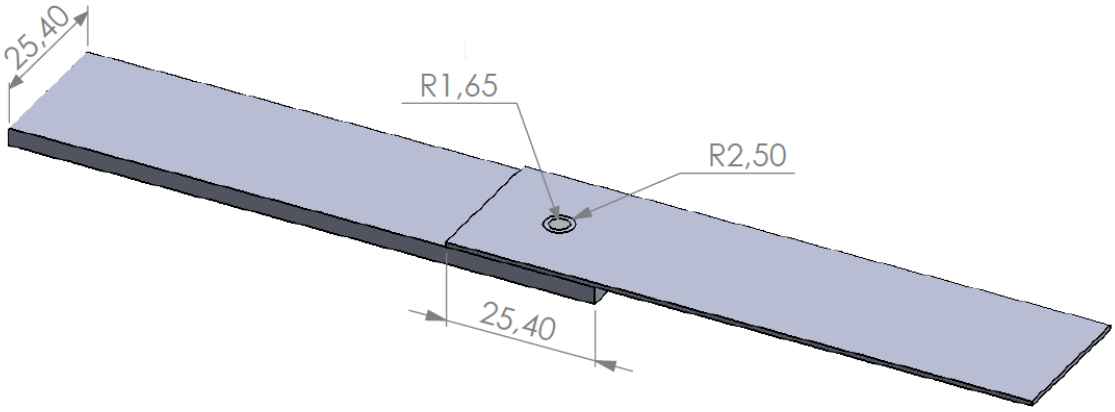

Figure 10 - Partially overlapped configuration for lap shear test (dimensions in mm).

To evaluate the feasibility of the weld using the smaller tool while simultaneously obtaining an adequate processing window, a screening experiment was performed. The One-Factor-At-a-Time methodology was used to evaluate six different parameters through a variety of ranges presented in RFSSW welding literature, and find a defect-free processing window.

Although often neglected in Refill FSSW research, working with a defect-free process window (that is, without major internal defects such as voids) is imperative to capture the purely metallurgical variation of the response with the variation of parameters. Failing to do so leads to an explanation of the process which is predominantly defect-based and is therefore shallower.

Once such a window was found, an appropriate design of experiments was chosen. The Box-Behnken Design is the most efficient design when it comes to the ratio between predictors on the model and the number of experiments [54]. This was a desired feature, once the supply of material for the welds was extremely limited due to logistic reasons involving transportation from China to Germany. In addition, it is better than the Taguchi Method to evaluate interactions when these are not previously known. This was the case due to the novel character of the research in terms of tool design and sheet configuration. It was also preferable over the Central Composite Design, once the high value chosen for Rotational Speed (3000 rpm) was the recommended limit for the machine,

rendering the axial points of this design (which are needed to grant rotatability) impossible to perform.

To fit the chosen design, the three most influential parameters according to the screening experiments were investigated in three levels (coded as -1, 0, and +1) over the desired processing window. These values and parameters are specified in Table 4. For the discarded variables, Clamping force was set to 10kN, no dwell time was used, and plunging time was a consequence of speed and rate.

Table 4 - Box-Behnken Design factors and levels, coded and uncoded.

Parameters	**Levels**		
	-1	***0***	***+1***
Plunge Depth [mm]	0.6	0.8	1.0
Rotation Speed [rpm]	1500	2250	3000
Plunge Speed [mm/s]	0.5	0.75	1.0

This method was used, at first, to analyze the process and to optimize the weld in terms of mechanical properties. Additionally, in a novel approach to aid in the comprehension stage of the process, microstructures for all 15 welding conditions required for the method were acquired. In possession of these, a few quantifiable microstructural features were measured and used as a response of the design to generate independent models. This was done after the optimization step and had the sole purpose of measuring the influence of process parameters in these features, as well as correlating them to the respective Lap Shear Strengths.

The Box-Behnken Design uses the least-squares method to develop a full-quadratic model fitting the experimental data. For that reason, it is often coupled with ANOVA to assess the validity of the model developed, given that this tool provides several statistical indicators to make such an evaluation. This analysis was also performed.

4.3.2 Mechanical Characterization

In order to assess the mechanical properties of the welds, the partially overlapped samples were submitted to lap shear testing, according to ASTM D3163-01 [58]. Tests were performed using a screw-driven Zwick Roell® 1484 machine, equipped with a 200 kN load cell at room temperature. Specimens were tested with a grip area of 25,4 x 25,4 mm² and 1mm/s test displacement rate. An offset between grips was necessary to guarantee the axial loading on the specimens and prevent any initial bending forces. All lap shear tests were performed 7 days after welding, once the alloys in the 2xxx series suffer natural aging at room temperature and hardening usually stabilizes after four days [14].

Aiming to get comprehensive information on the samples, microhardness maps were collected in a Struers DuraScan® 70 G5 machine. These maps were designed in agreement with ASTM Standards [59, 60] utilizing the Vickers method, with 100g of main load, 15 seconds of dwell time and 0,1mm spacing in between indentations in all directions. To assess the natural aging effect, several samples were welded on the same day and hardness maps were acquired for the samples in different aging conditions: as-welded, 4 days, 7 days, and 30 days after welding.

4.3.3 Thermal Cycle

To observe the thermal cycle inherent to the process, two methods were used: Thermocouple and Infrared Camera. Using thermocouples is the most established temperature measurement approach in Refill FSSW research and allows for a good comparison with the literature. Infrared Camera compliments that analysis with a precise measurement of the surface of the sheets, which enables comparison with the temperatures reached inside the sheets while also providing a different perspective on the measurement process.

In the thermocouple analysis, four K-type thermocouples were positioned by drilling holes in the bottom surface of the weld-to-be. The positions of the holes were chosen carefully based on the desired analysis. One thermocouple was positioned in the center of the weld, given the importance of this position for modeling purposes. The second was positioned 2.5 mm away from the center of

the weld, underneath the sleeve, to evaluate at which temperatures the deformation is not enough to promote full dynamic recrystallization, consequently forming the TMAZ. The third was positioned 5 mm away from the center of the weld, where the microstructure transitions from HAZ to BM, to observe the maximum temperature reached before precipitates start to grow. The last thermocouple was positioned 9 mm away from the weld center, outside the clamping ring region, so that a comparison could be drawn between temperatures measured into the weld and on the surface (through Infrared camera). The depth of the tip of the thermocouples was always equal to the Plunge Depth reached by the process, to make sure that plunging would not destroy the thermocouples, and facilitate comparison between conditions. A diagram representing this positioning is depicted in Figure 11.

Simultaneously, the process was captured using an INFRATEC ImageIR 8300® and spraying Dupli-Color Lackspray Tuning Supertherm Black on the sheets. This allowed a video to be recorded and the surface distribution temperature over time to be observed aided by the software IRBIS3 Professional®.

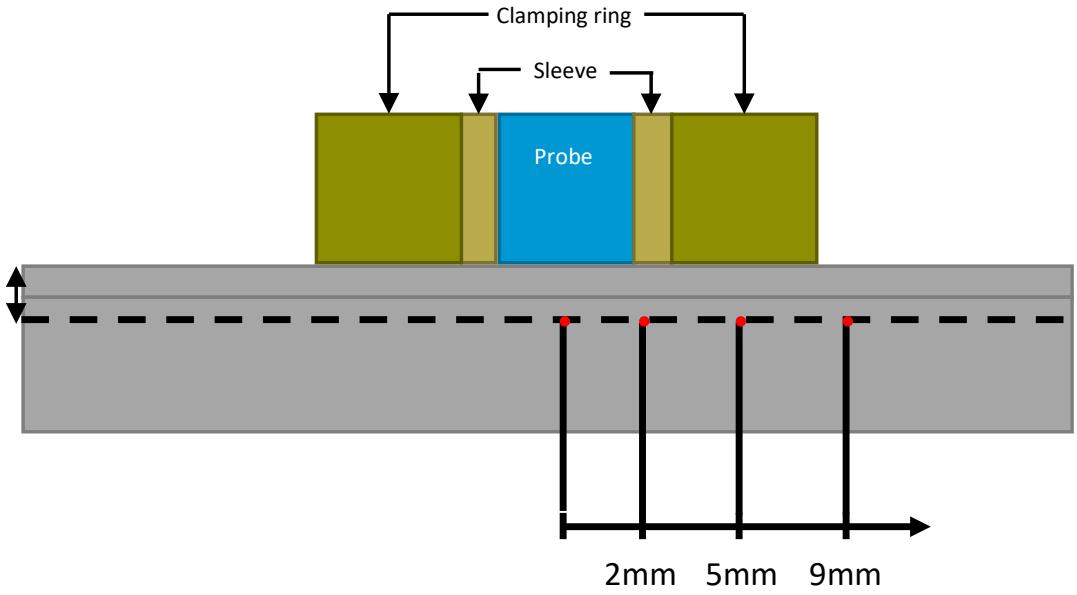

Figure 11 - Thermocouple positioning diagram. The dashed line represents Plunge Depth, which varies with welding condition.

4.3.4 Microstructural Characterization

Microstructural analyses for the screening experiments, statistical investigation and failure type characterization were carried out with a LEICA SM IRM® optical microscope during the stage of weld production. More extensive confirmatory analyses were performed with an Olympus BX41M-LED ® optical microscope and Olympus DP 21® embedded camera. Furthermore, additional investigation was performed using a FEI Quanta 400 FEG Scanning Electron Microscope.

All microstructural characterization is preceded by standard metallographic preparation according to ASTM E3. Welds are cut and embedded in transparent epoxy resin. Then samples are ground and polished using SiC foil and successive polishing cloths in a Struers TegraPol-31® until the central plane of the weld is reached

4.3.5 Tool Wear Characterization

To assess the wear progression on the adjustable shoulder, three wear conditions of interest were established based on previous research using the reduced dimensions tool: new tool (I), tool after 15 welds performed (II), and after 200 welds performed (III). The toolset was removed from the machine and cleaned every 15 welds using an aqueous NaOH solution heated to 40°C for 2 hours.

The modifications on the shoulder's visual aspect due to wear at each condition were observed under a VHX-6000® digital microscope. The deformation at the tip of the shoulder, which is the surface of initial contact between tool and sheets, was observed and measured by a Keyence VK-9700® Violet Laser Color 3D Laser Scanning Confocal Microscope, and results were analyzed using the VK-Analyzer software bundle.

5 RESULT AND DISCUSSION

5.1 Process analysis

To properly optimize the Refill Friction Stir Spot Welding process for the combination studied, a screening experiment was conducted to find a defect-free processing window. The variables analyzed were Clamping Force, Dwell Time, Plunge/Retract Speed, Plunge/Retract Time, Plunge Depth and Rotational Speed.

This screening experiment revealed that the most influential variables on the process were Rotation Speed, Plunge Depth and Plunge/Retract Speed (henceforth referred to interchangeably as Plunge Speed or Rate) and thus, those were the variables chose for the statistical model. Their ranges of interest were established, using the same defect-free criteria as before, and the next step of the optimization was conducted as previously described in Table 4.

5.1.1 Process Optimization

The Box-Behnken Method was applied, and the chosen response variable was Lap Shear Strength. Samples were randomly tested and the obtained responses are presented in Table 5. These results were analyzed in Minitab®.

Initially, it is important to note that all samples far surpassed the requirements for RSW in aerospace applications from the AWS D17.2 [46], which is 1.45kN on average.

Table 5 - Order and responses for samples of the Box-Behnken Design.

Std Order	Run Order	Plunge Depth [mm]	Plunge Speed [mm/s]	Rotational Speed [rpm]	Lap Shear Strength [N]
5	1	0,6	0,75	1500	2908,82
10	2	0,8	1	1500	2867,49
9	3	0,8	0,5	1500	3194,14
3	4	0,6	1	2250	2547,14
15	5	0,8	0,75	2250	3533,21
6	6	1	0,75	1500	3550,52
13	7	0,8	0,75	2250	3347,21
14	8	0,8	0,75	2250	3591,31
8	9	1	0,75	3000	2853,89
12	10	0,8	1	3000	3454,60
4	11	1	1	2250	3718,31
2	12	1	0,5	2250	2833,85
11	13	0,8	0,5	3000	2871,49
7	14	0,6	0,75	3000	2179,04
1	15	0,6	0,5	2250	2731,55

First, a full-quadratic model was used to fit the responses. The ANOVA for this model, presented and discussed in APPENDIX A, revealed terms with no statistical significance. These terms were removed from the model and a new ANOVA was performed. This process is referred to as backwards elimination of terms, and considerably improved the quality of the model.

The adequacy of the model was checked, and the model presented itself as satisfactory. The adequacy analysis is thoroughly described in APPENDIX B. The ANOVA analysis can be summarized in Figure 12, showing the Degrees of Freedom (DF), Sums of Squares (SS), Means Squares (MS) for each term, which are used to calculate the F-value. Aside from this statistic, used to determine significance, an approximation of the percentage contribution of each term is shown, along with the p-value. The p-value approach, paired with critical judgment, was used to draw statistical conclusions with 95% confidence.

Analysis of Variance

Source	DF	Seq SS	Contribution	Adj SS	Adj MS	F-Value	P-Value
Model	8	2352139	85,00%	2352139	294017	4,25	0,047
Linear	3	1121655	40,53%	1121655	373885	5,41	0,038
Plunge Depth	1	838525	30,30%	838525	838525	12,12	0,013
Plunge Rate	1	114364	4,13%	114364	114364	1,65	0,246
Rotational Speed	1	168766	6,10%	168766	168766	2,44	0,169
Square	3	737947	26,67%	737947	245982	3,56	0,087
Plunge Depth*Plunge Depth	1	457976	16,55%	528586	528586	7,64	0,033
Plunge Rate*Plunge Rate	1	68806	2,49%	88137	88137	1,27	0,302
Rotational Speed*Rotational Speed	1	211166	7,63%	211166	211166	3,05	0,131
2-Way Interaction	2	492537	17,80%	492537	246268	3,56	0,096
Plunge Depth*Plunge Rate	1	285621	10,32%	285621	285621	4,13	0,088
Plunge Rate*Rotational Speed	1	206916	7,48%	206916	206916	2,99	0,134
Error	6	415002	15,00%	415002	69167		
Lack-of-Fit	4	382483	13,82%	382483	95621	5,88	0,151
Pure Error	2	32519	1,18%	32519	16259		
Total	14	2767141	100,00%				

Model Summary

S	R-sq	R-sq(adj)	PRESS	R-sq(pred)
262,996	85,00%	65,01%	4043932	0,00%

Figure 12 - ANOVA table and model summary.

It can be seen directly from the table that the p-value for the model is $p = 0{,}047$ (slightly under 0,05). This leads to the conclusion that the model can statistically explain variation in the response with 95% confidence. The lack-of-fit presented a p-value of $p = 0{,}115$, which is satisfactory, given that even if a lower confidence level was chosen (90%), this value would not be significant. In addition, the percentage contribution of the errors was satisfactory small (1,18%).

The R² value of 85%, shown in the model summary, is considered satisfactory for Box-Behnken Design and essentially means that the model used can explain 85% of the variation in the response.

The Adjusted-R² is lower than the R², as expected. This happens because increasing the number of predictors in any given model always increases the R² value. The Adjusted-R², on the other hand, is less biased. Thus, this difference between these two statistics in a model is indicative that the model is slightly over-fitted. The 20% difference in this case is not neglectable, but also not big enough to discard the model.

The over-fit is corroborated by the Predictive-R² value of 0%. The Predictive-R² statistic is calculated by removing one observation from the model and trying to fit it into the model generated by the other 14 observations. Therefore, a low or negative value is also indicative of either over-fit or differences between the overall behavior of the response when compared to the sample size investigated.

However, the Adjusted-R² is still an improvement from the full-quadratic model initially performed and is sufficiently close to R² to consider the model adequate, given all the other adequacy checking performed.

Having interpreted the model, the following equation was used to map the response, where PD stands for Plunge Depth, PR for Plunge Rate/Speed and RS for Rotational Speed:

$$Lap\ Shear\ Strength = -2070 + 12745\ PD - 2818\ PR + 0{,}81\ RS - 9459\ PD^2 - 2472\ PR^2 - 0{,}000425\ RS^2 + 5344\ PD * PR + 1{,}213\ PR * RS$$

To better visualize this equation, contour plots were drawn, and are shown in

Figure 13. In Figure 13(A), Plunge Rate is fixed at 0.75mm/s and it is possible to observe the variation in LSS as a function of Rotational Speed and Plunge Depth. In Figure 13 (B) and (C), Rotational Speed and Plunge Depth are fixed, respectively, and the remaining variables are shown on the plot. The

corresponding response surfaces along with additional data from the Box-Behnken analysis are shown in APPENDIX C.

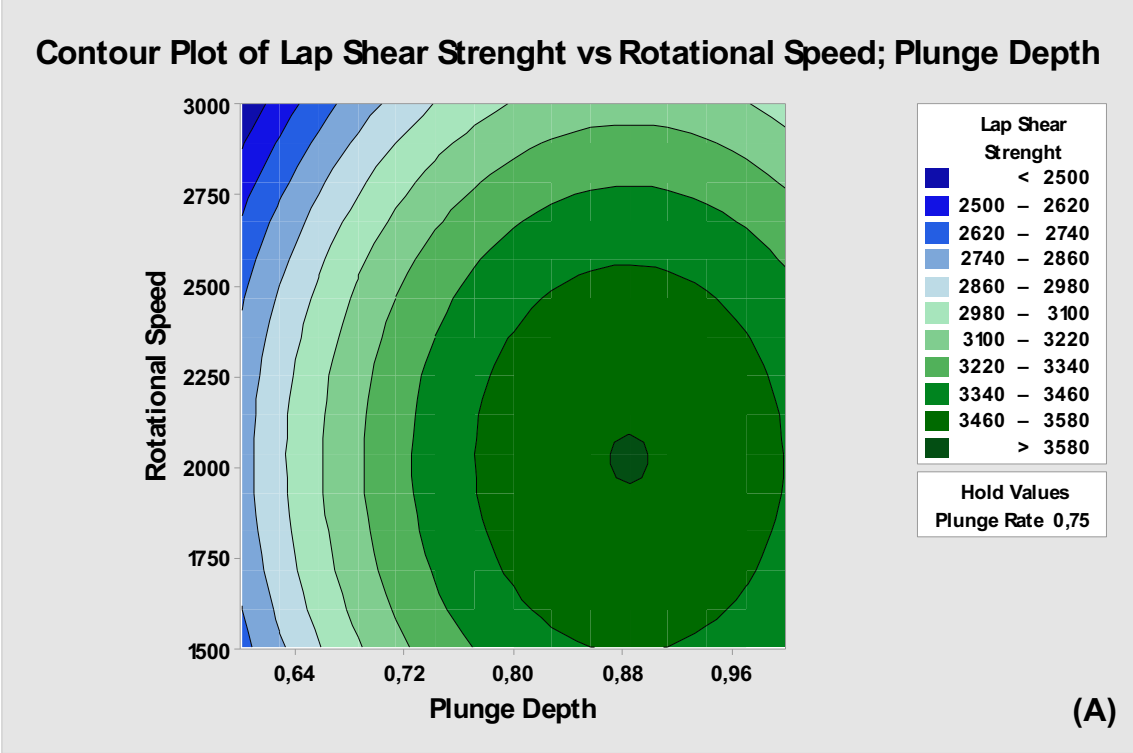

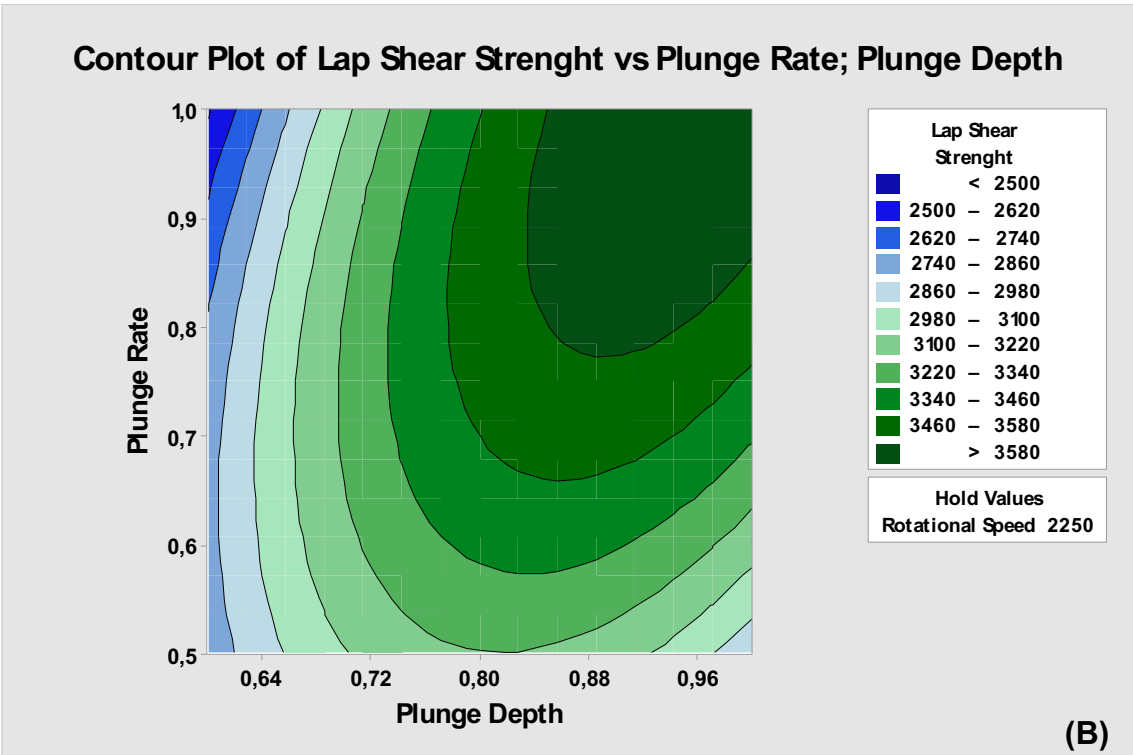

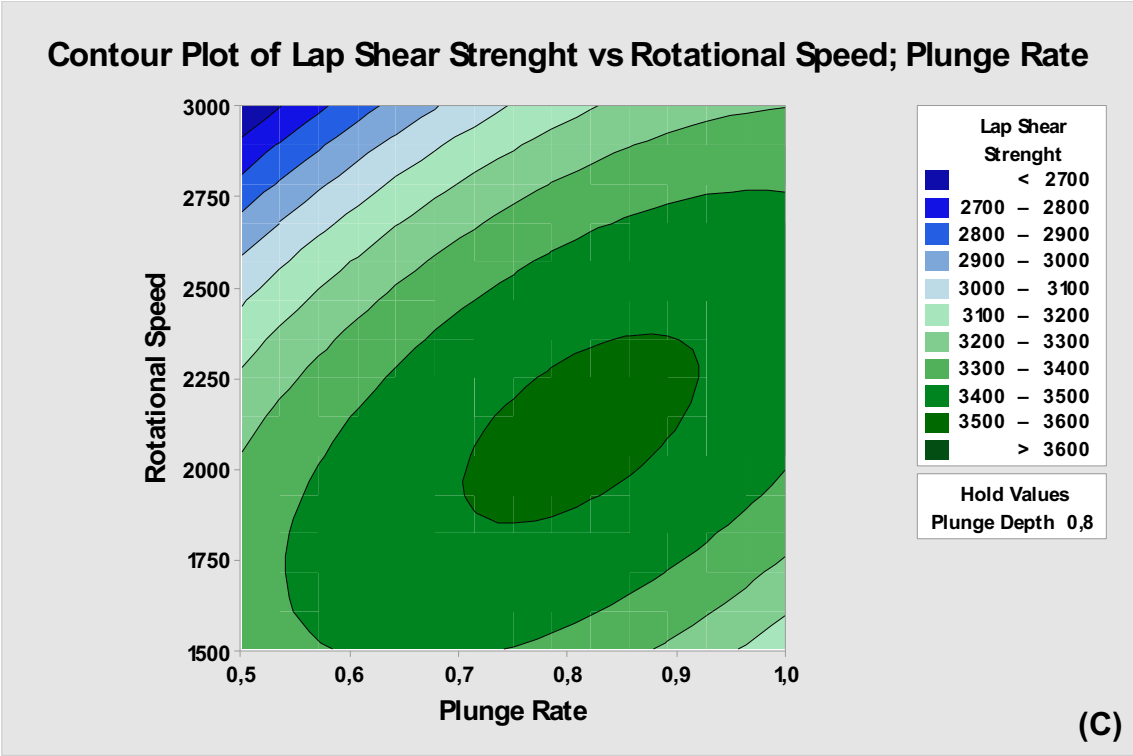

Figure 13 - Contour Plots for the equation generated by the Box-Behnken model.

Aside from describing the overall behavior of Lap Shear Strength as a function of the selected variables, the model generated allows for prediction of an optimal response. This is done through deriving the equation and equaling the derivative to zero, finding a global maximum.

Figure 14 shows a theoretical optimal condition of 3.69kN with parameters set at 2378.78 rpm Rotational Speed, 0.9556 Plunge Depth and 1mm/s Plunge Speed (which is the maximum value studied).

It is important to point out that no additional tests outside of the processing window to check for further increase in strength were carried out. This decision was made given that said window was defined on the parameter limits with which the process produces defect-free welds.

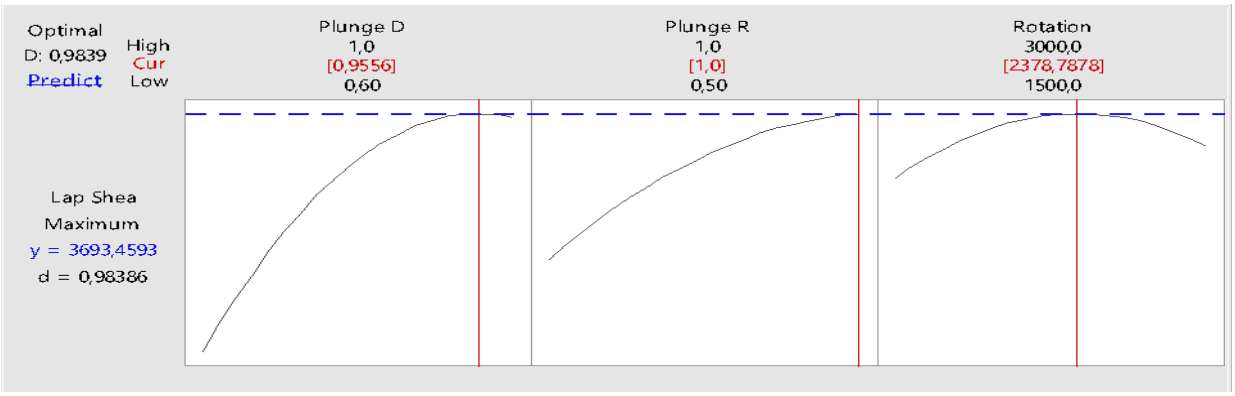

Figure 14 - Optimal response predicted by the design.

Confirmation runs were performed with the goal of assessing the real optimized strength of the weld, once the model is theoretical and, for several applications, fails to come close to the real strength value.

The measured value of 3.2±0.1kN was extremely satisfactory, once 90% of the theoretical strength was attained. Additionally, this mean strength evidently surpasses the mentioned requirement for resistance spot welding with equivalent thickness for aerospace applications established by the American Welding Society (AWS) [46], which is 1.4kN.

5.1.2 Parameter Influence

After optimizing the model and obtaining the conditions necessary for a weld with maximum strength, it is useful to assess which parameters most influence the process (that is, with a small variation in the parameter, a significant variation in response is observed). This can aid when performing similar tests in different material combinations, as well as contribute to adjust the process when other processing conditions change. Additionally, it provides a statistical basis for behaviors that are sometimes empirically observed.

Among the parameters and their interactions, it is observable from the ANOVA table in Figure 12 that the only ones that can be considered statistically significant with 95% confidence (that is, having a p-value inferior to 0,05) are Plunge Depth and its square term (PD²). The interaction Plunge Depth * Plunge Rate has a p-value of $p = 0{,}088$, and thus should also be given attention. This value is sufficiently close to 0,05 to consider the interaction slightly significant,

once in would have significant p-value if 90% confidence were required. The choice of this confidence is arbitrary, thus, subject to interpretation.

To enhance visualization quality, is it useful to draw a Pareto Chat of the parameters and their respective effects. This chart is presented in Figure 15, where the significant effects are highlighted in green. It can be seen from the chart that while Plunge Depth is the most significant parameter to Lap Shear Strength, Plunge Speed seems to be the least influential, opening up the possibility to study faster processing times in future investigations.

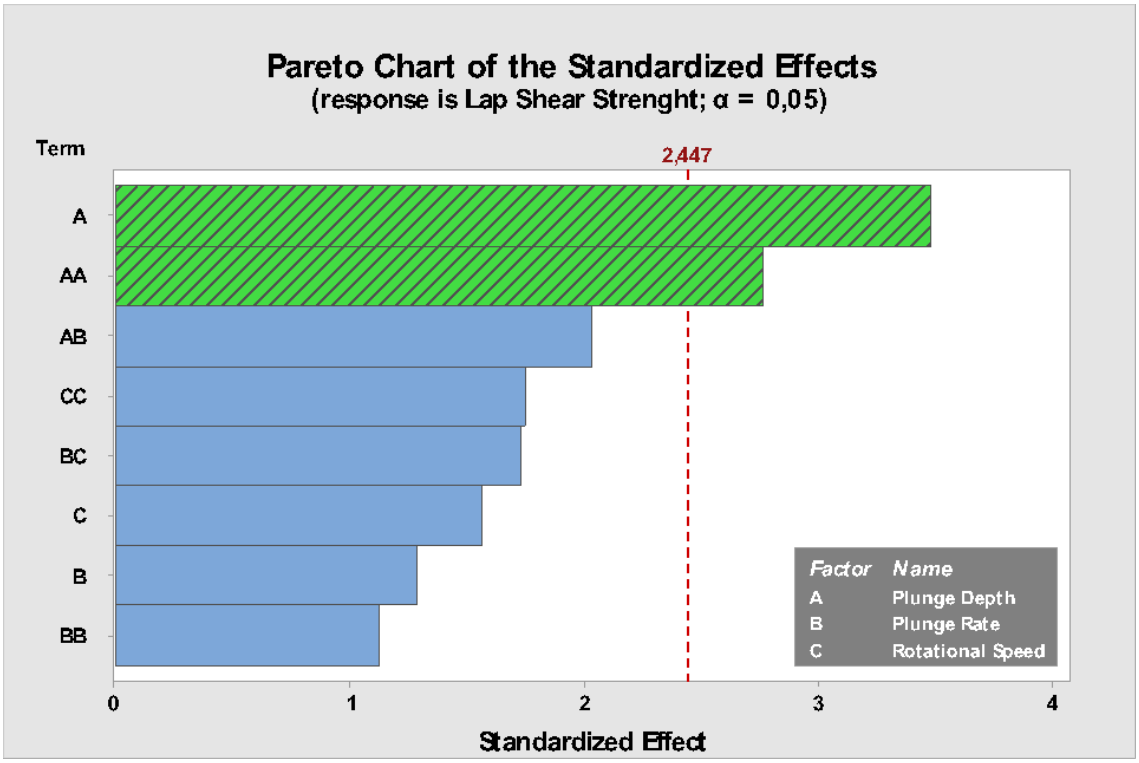

Figure 15 - Pareto Chart of the Standardized Effects.

The influence of the parameters on Lap Shear Strength was straightforwardly derived from the optimization model. These same parameters, however, may influence microstructural features that do not impact Lap Shear Strength directly, but may be important for other considerations.

Usually, microstructural features are investigated on the optimized sample only, and sometimes new statistical analysis, such as OFAT, is conducted to infer how parameters influence those features. Using the same processing window

and statistical methodology, however, provides more information on the behavior through the whole extension of the processing window.

With this in mind, the same conditions used in the box Behnken design for lap shear optimization were used to produce samples for microstructural inspection. Once microstructures were captured, quantifiable features present in the weld were measured and used as responses from the model. This allowed an ANOVA analysis to be carried out, which in turn provided information on which process parameters are related to which parts of the microstructure.

It is important to point out that the same adequacy checking described for the mechanical properties analysis was used in this step for every single feature measured. The models that did not satisfy the adequacy conditions were immediately discarded. The measured features which presented the largest significance to their respective model were Hook, Bonded Width and Layer Width, these models are described in a summary presented in Table 6. These features are also drawn on Figure 16.

The hook feature is well-known and thoroughly described in the literature [5, 27, 30, 36], albeit different authors give different explanations to its formation and effects. This feature was measured here by drawing an imaginary extension of the interface between the sheets and measuring the height of the tip of the hook.

Another well-established feature in Refill FSSW is the Bonded Width [5, 21, 30, 36]. Even though authors also diverge in a few aspects regarding the measurement of this feature, simplifying this width as the horizontal distance between the hook tips on both sides proved to be sufficient to obtain a good model.

In all samples, a distorted layer can be observed in the center of the stir zone. This happens because the former aluminum cladding (pure aluminum) of the sheets is mixed and welded to the alloy on both sheets. Due to process time and temperature, however, not enough energy is provided to make the composition homogeneous in this region. This ultimately means that diffusion is enough to promote joining, but this region remains rich in aluminum, and

consequently solute poor, which causes it to play an important role during loading, as will be further explained.

The presence of a notch on the surface of the weld was also observed, which is further discussed in the Tool Wear section. All the features can be observed in the microstructure of the optimized weld, shown in Figure 16a. In this figure, Bonded Width is represented by the full line (B), while Layer Width is represented by the dashed line (L). Hook Height is indicated (h) in the Figure 16b in higher magnification.

Microstructural variants obtained during this study are shown for comparison in Figure 17. It can be evidently seen from Layer Width, for example, that differences in these features are stark with varying parameters.

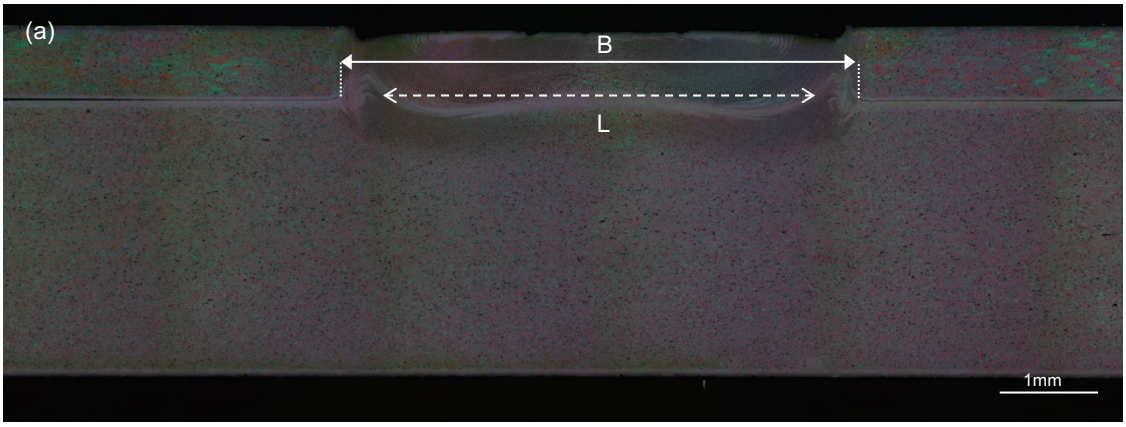

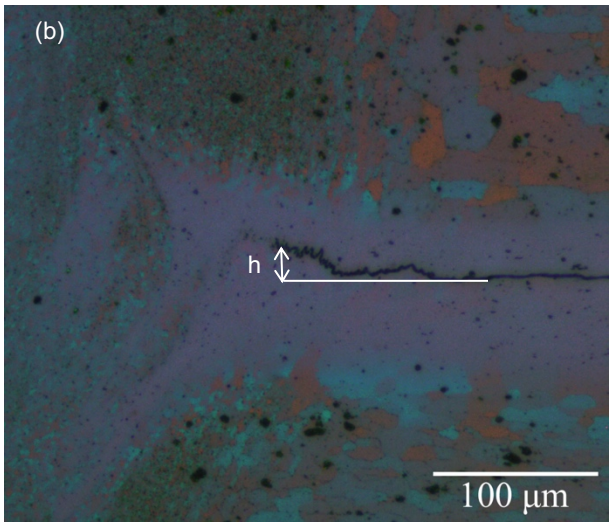

Figure 16 - Microstructures of (a) optimized welding condition; (b) Hook region for this condition, with hook height “h” indicated. In (a) the full line is indicative of Bonded Width (B) while the dashed line indicates Layer Width (L).

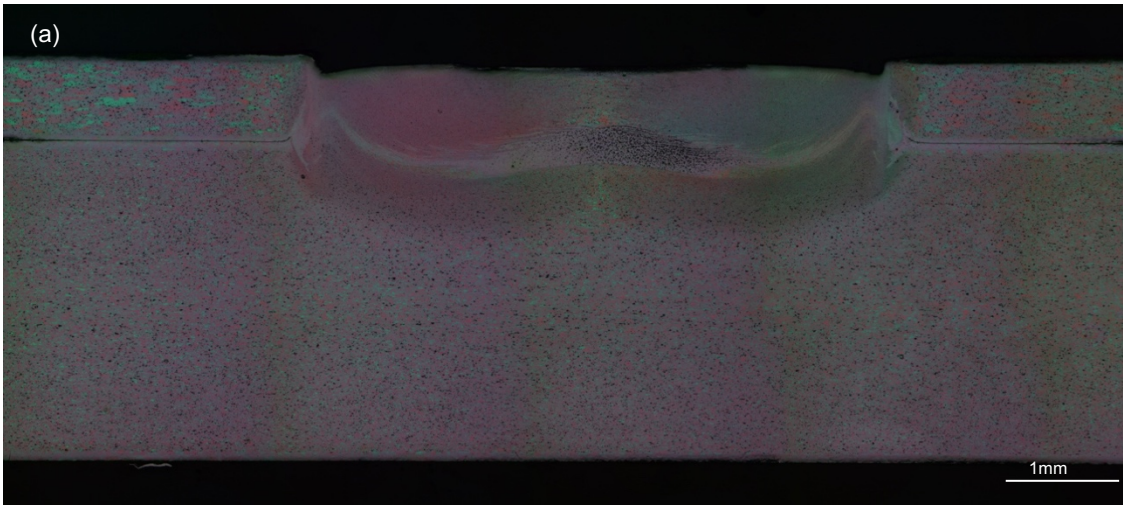

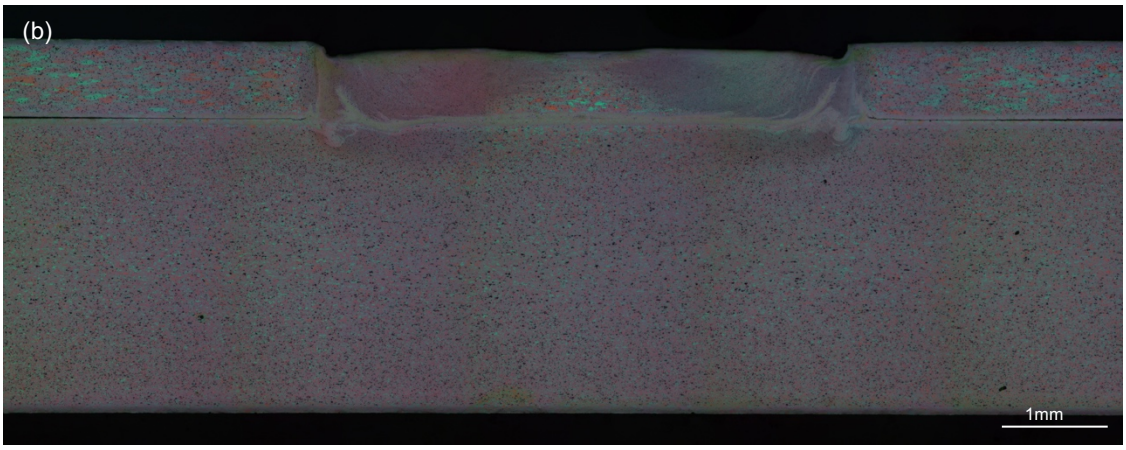

Figure 17 - Microstructures of (b) Higher Plunge Depth variation; (c) Lower Plunge Depth variation.

Alongside each model’s equation, Table 6 presents the model’s R^2 and R^2_{adj} values, the process parameters with the first and second highest influence according to the ANOVA model.

Table 6 - Summary of the ANOVA analysis on some microstructural features.

Feature	Model R^2/R^2_{adj}	Main influence	Second highest influence
Hook	84%/71%	Rotational Speed	Rotational Speed^2
Equation	*Hook height [µm]= -12.8 -70.5PD-64.6PR+0.0564RS-0.000021RS^2+0.0454PD*RS+0.0228PR*RS*		
Bonded Width	92%/88%	Plunge Depth	None
Equation	*Bonded Width [µm] =2698+3581PD-129.7PR+0.2684RS-1405PD^2-0.36PD*RS*		
Layer Width	82%/64%	Plunge Depth	Plunge Depth^2 and Plunge Rate
Equation	*Layer Width [µm] = 6925-5195PD-3256PR+0.77RS +0.000365RS^2+7685PD*PR-2.17PD*RS-0.94PR*RS*		

With these equations in hand, aside from having statistical support to explain how parameters influence microstructure, it is possible to observe how these features influence mechanical properties, giving a better understanding of the processing-microstructure-properties relationships.

Bonded Width plays an important role in interfacial shear (through-the-weld) failure, for example, once an increased bonded width increases the area bearing loading, so it is positively correlated to Lap Shear Strength, as shown in Figure 18. This feature is mostly determined by the Plunge Depth, as described in the model in Table 6, and therefore explains why Plunge Depth is a significant variable for Lap Shear Strength.

The same rationale can be applied to Layer Width. According to the model, increasing Plunge Depth generally decreases Layer Width. Given that this layer is solute poor and plays an important role in the mechanical behavior of the welds, as further explained in following sections, it is expected to affect Lap Shear Strength. Therefore, higher Plunge Depths cause Layer Width to decrease, and LSS to increase.

Hook height, on the other hand, interestingly showed no significant influence on Lap Shear Strength, probably due to the small variance in size when compared to the thickness of the top sheet. In Table 6, the equation shows that

hook height was mainly influenced by Rotational Speed. This suggests that even though Rotational Speed does influence the microstructure of the resulting weld, since the hook is not influential in Lap Shear Strength, its influence is diminished in the LSS model.

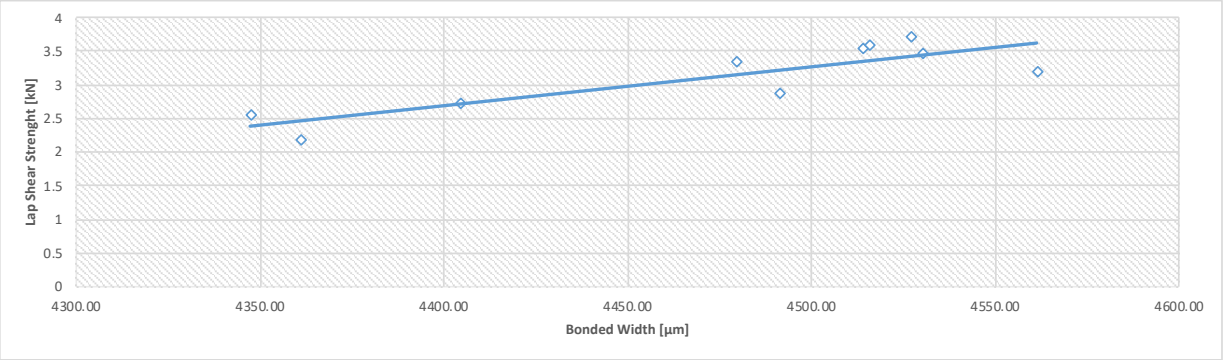

Figure 18 - Correlation between Bonded Width and Lap Shear Strength.

5.2 Mechanical Behavior

The Lap Shear tests performed during the optimization stage presented two fracture modes. The macroscopic aspect of the fractures can be observed in Figure 19 and their respective cross-sections can be observed in Figure 20.

The fracture shown on the right-hand side happened in 66.6% of cases. In this case, crack propagates in a shear mode parallel to the original interface between sheets and is therefore referred to as Through-the-weld or Interfacial Shear fracture. The fracture on the left-hand side happened on the other 33.3% of cases and presents a crack propagating perpendicular to the original interface, leaving the stir zone (weld nugget) attached to the bottom sheet. This mode will be referred to as pullout mode. The optimized condition fractured presented pullout fracture in all samples.

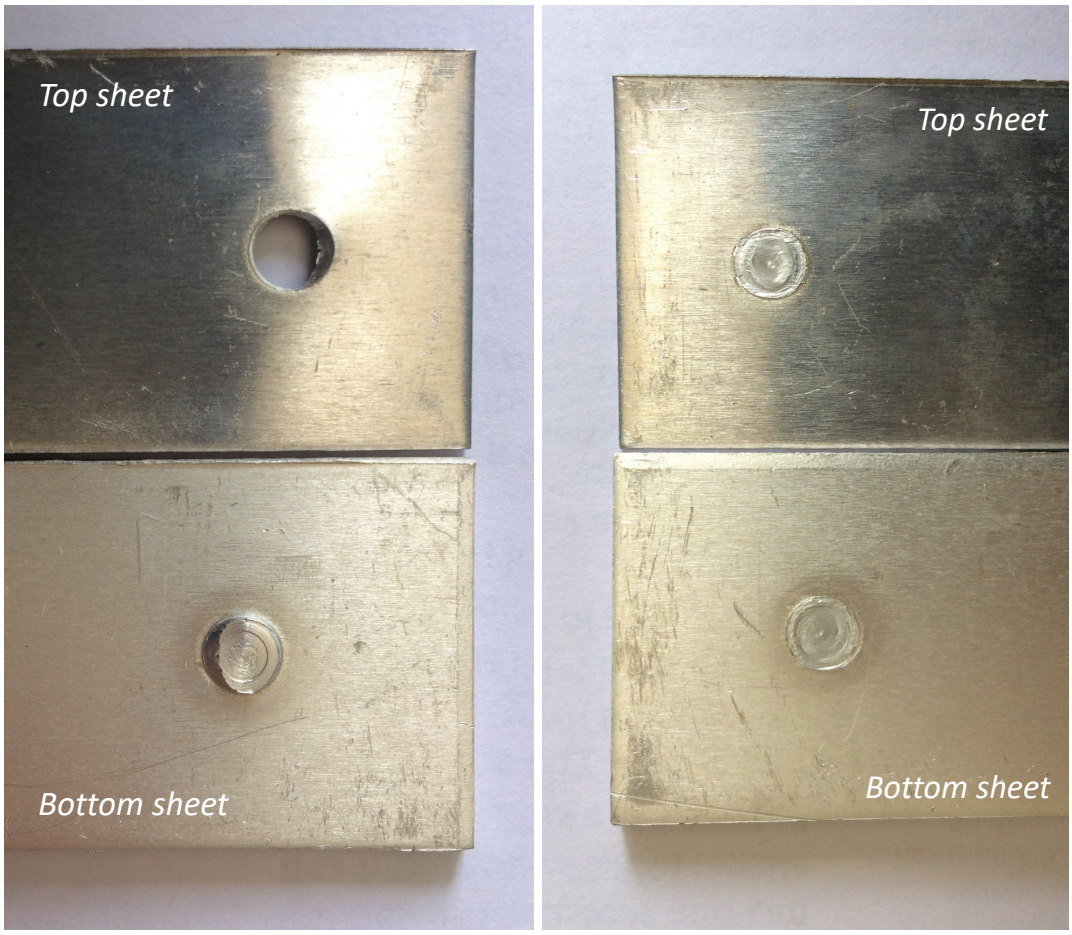

Figure 19 - Two different fracture modes observed: Pullout on the left-hand side and Through the Weld on the right-hand side.

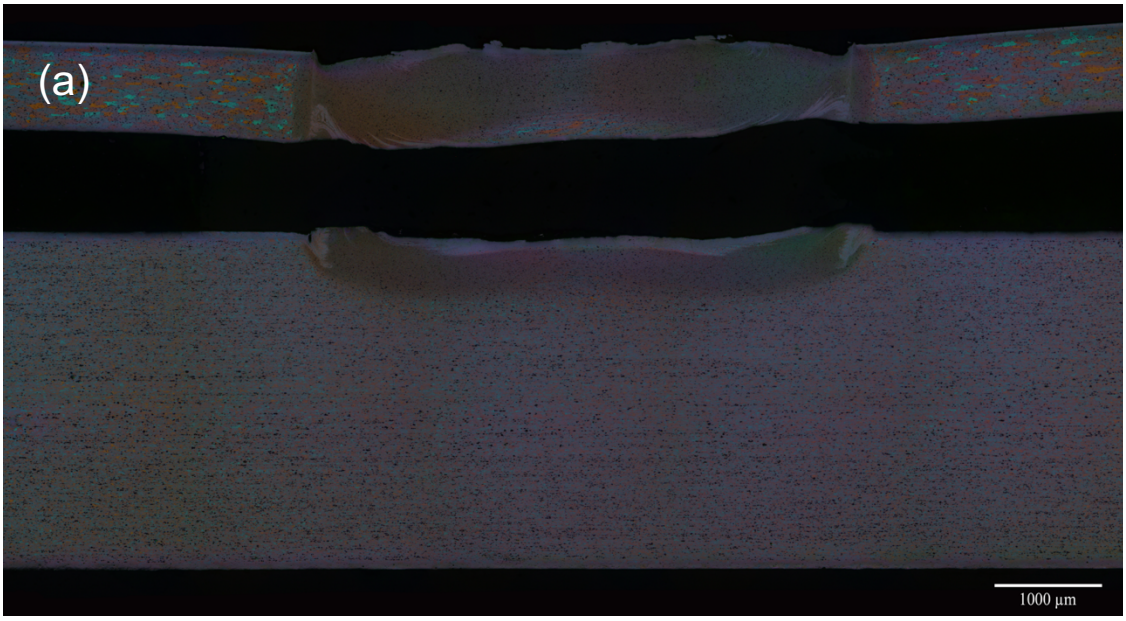

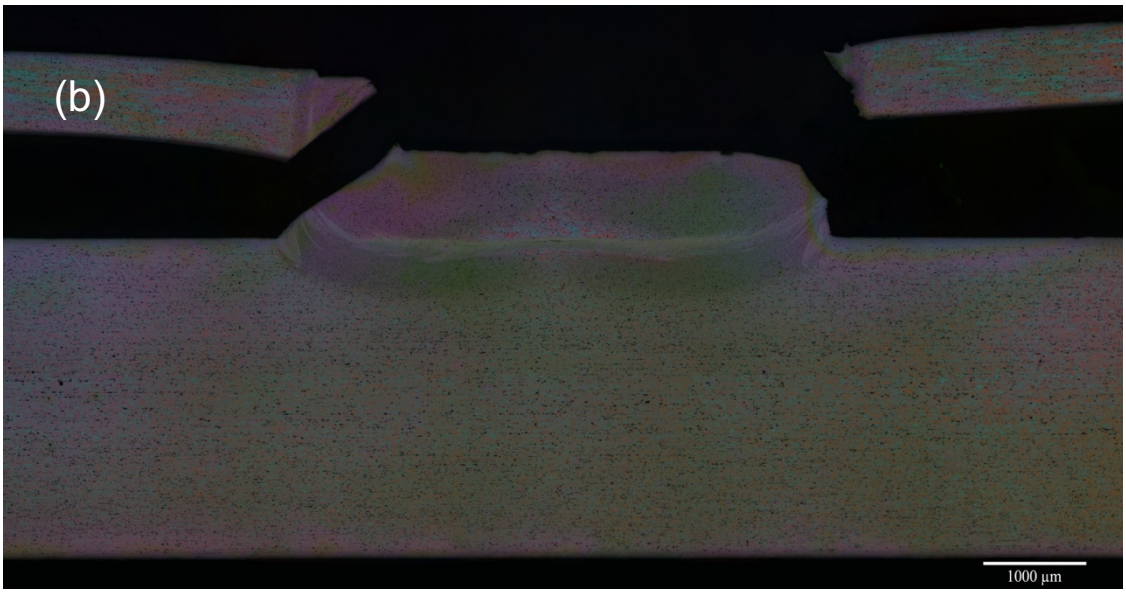

Figure 20 - Cross-section of the two fracture modes (a) Through the Weld and (b) Pullout.

Both fracture types have been previously reported in the literature [5, 6, 27, 34] with minor differences depending on the alloy studied. Observing Alclad-AA2024, Li et al [6] reported four different fracture modes, depicted in Figure 21. In that study, however, one of the modes is associated with high dwell times (Figure 21c) and one shows propagation in the top and bottom sheet simultaneously (Figure 21d). It is natural that neither occurred in this project, given the fact that no dwell time was used and the bottom sheet is almost four times thicker than the top sheet, rendering propagation through the bottom sheet extremely unlikely.

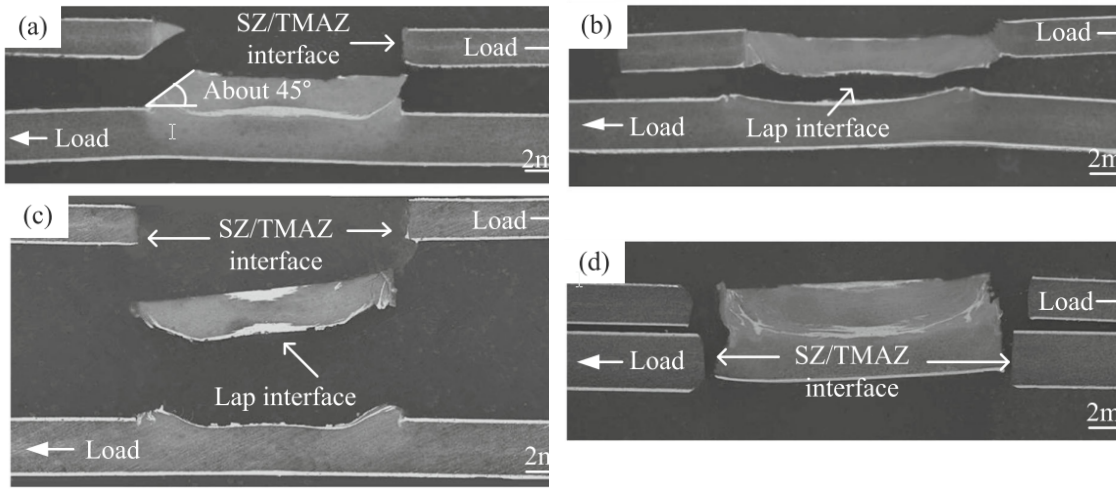

Figure 21 - Fracture modes reported in AA2024 by Li et al. [61].

This pointed to an agreement between the observed fracture modes (Figure 20) and current literature (Figure 21 a and b). At first, a correlation between fracture mode and process parameters, as well as process response, was sought. However, it was not possible from experimental data to state any particular relationship. This investigation is presented in detail in APPENDIX D.

In an initial effort to understand crack initiation and propagation, loading-unloading experiments were performed. These experiments involved loading a specimen and subsequently removing the load. This was done in increasing loading steps.

Additionally, microstructure samples were taken stopping the tensile test at several loading points and evaluating the specimen's cross-section. The Load-Displacement curves from the cyclic portion of the test are depicted in Figure 22.

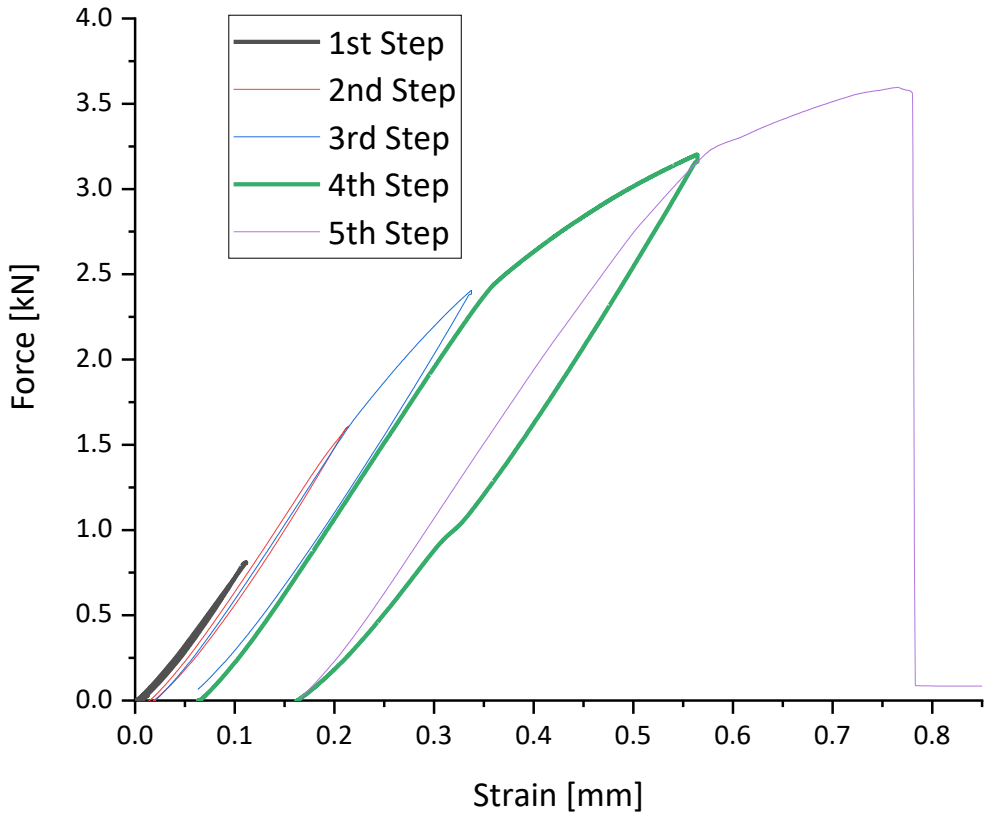

Figure 22 - Loading-Unloading tensile test curves on cyclic loading.

The hook regions from the cross-section of the highlighted curves, (800N and 3200N) are shown in Figure 23. When evaluating this region, it can be observed that plastic deformation happens around the hook due to its stress concentrating nature, already extensively described in the literature [5, 27, 30, 36].

Combining this observation with the mechanism presented by Li et al. [6] leads to believe that crack initiates in this spot and propagates through one of two regions: the former Aluminum cladding layer in the center of the weld or the Stir Zone/Thermomechanically Affected Zone interface.

The aluminum cladding is a 99% aluminum coating that end up mixed inside the stir zone after welding. As previously mentioned, due to process time and temperature, not enough energy is provided for complete diffusion to take place and homogeneity in composition to be reached, and the remaining layer in the middle of the weld remains solute poor, offering less resistance for crack propagation.

The Stir Zone/Thermomechanically Affected Zone interface, on the other hand, is formed during the retracting stage. In this stage, the SZ is bonded to the TMAZ by diffusion. Given that this is the last stage of the process, the exposure to diffusion-promoting temperatures happens for a short period of time. This causes the region to have inferior mechanical properties when compared to the center of the Stir Zone and makes it a preferable path for crack propagation. Additionally, due to the aluminum’s high ductility, it is possible that some of the aluminum on the cladding gets pushed out from the center of the weld and into this region. This, however, needs to be further investigated before assertive conclusions can be drawn.

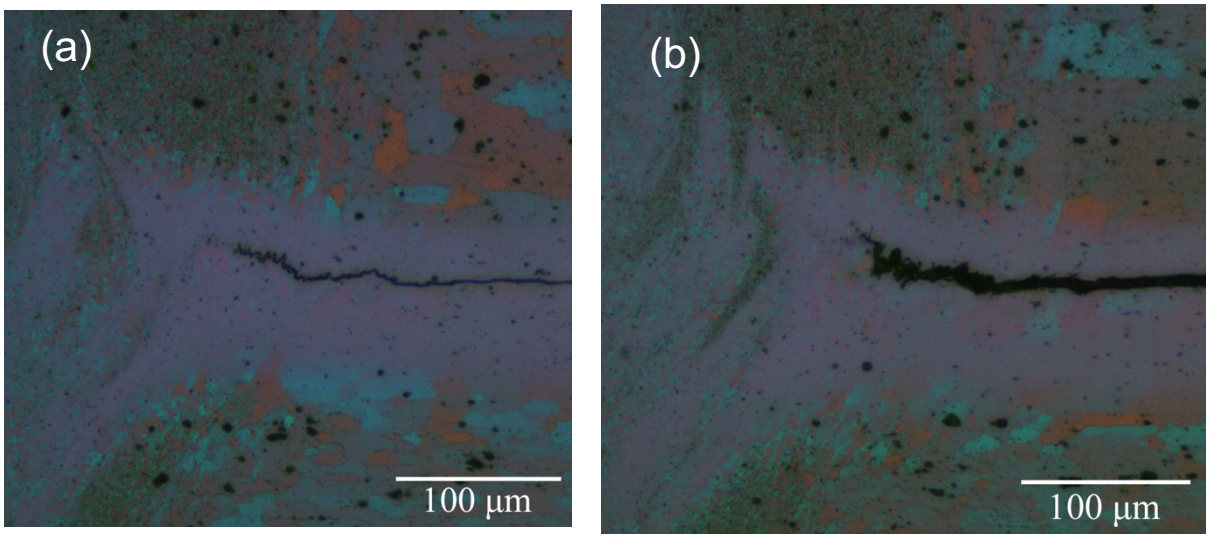

Figure 23 - Hook region on the right-hand size samples loaded to (a) 800N and (b) 3200N.

5.3 Thermal Cycle and Natural Aging

5.3.1 Thermal Cycle

The thermal cycle experienced by the optimized process was measured with four thermocouples, and is displayed in Figure 24. The maximum temperature reached was 434ºC and corresponds to approximately 70~75% of the material's melting temperature. As expected, this temperature is reached in the center of the weld. The different curves show thermocouples positioned with increasing distances from the center, which implies in a lower maximum temperature reached.

The maximum temperature captured by the IR camera was 220ºC. This temperature was registered on the edge of the tool; therefore, it is located at approximately 9mm from the weld center. The thermocouple positioned at this distance registered a maximum temperature of 221ºC. This indicates that due to the small thickness of the top sheet, superficial temperatures are relatively close to the temperatures on the interface of the sheets.

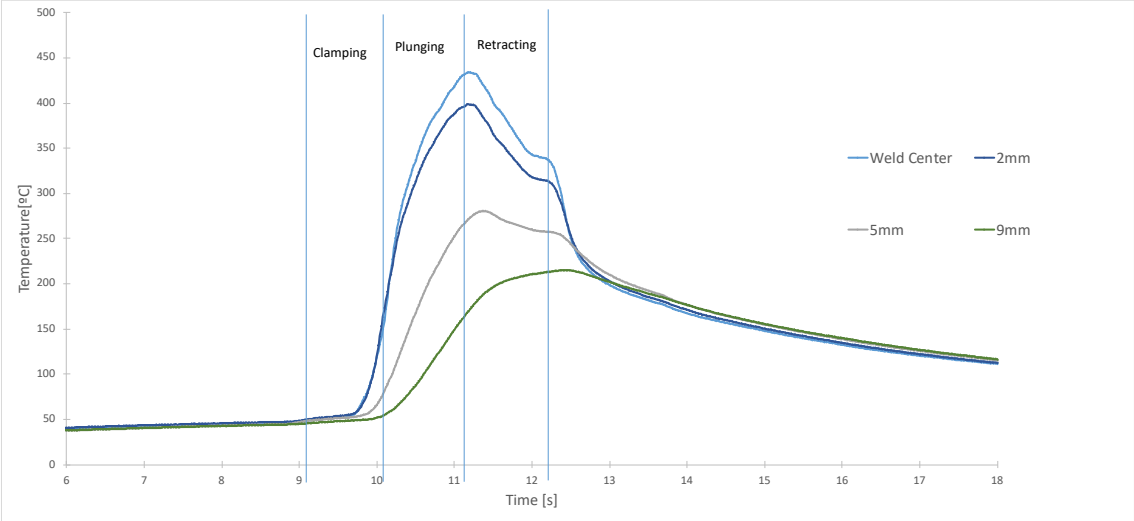

Figure 24 - Thermal Cycle experienced in four points along the aluminum sheet.

Additionally, the maximum temperature reached by the second thermocouple (2mm) was 398ºC. This thermocouple is positioned on the edge of the stir zone, suggesting that temperatures above 398ºC (reached inside the stir zone) are enough to promote full dynamic recrystallization, while lower temperatures (reached outsize the stir zone) promote only partial recrystallization.

Finally, the third thermocouple is positioned at 5mm of the weld center. This region marks the transition between HAZ and BM, as will be presented briefly. This indicates that temperatures below 280ºC do not promote any overaging of precipitates, preserving BM characteristics.

The main process steps are also depicted in Figure 24. It can be observed that temperature starts to increase during the clamping stage, as the rotating probe and shoulder touch the surface of the to-be-welded sheets. This increase happens at a faster rate in the center of the weld, and this tendency is maintained throughout the process. This is likely due to the lack of directions of heat extraction, when compared to outer regions of the weld.

During the plunging stage, heating becomes more intense, with peak temperatures at the end of the stage, as is usual for this process. Cooling starts during the retracting stage and the cooling rate increases significantly once the tool is removed.

5.3.2 Natural Aging

Knowing that 2xxx series aluminum alloys age naturally, every experiment performed in this project was carefully timed in order to guarantee repeatability and reliability. It is important to understand if and how natural aging affects mechanical properties, because ignoring this may lead to differences in the observed response (Lap Shear Strength, for example) to be misinterpreted as the effect of other variations in the process.

Until this point, no work containing the influence of natural aging on the mechanical properties was found. Therefore, this work included an evaluation on the post-processing natural aging of the welds. This evaluation happened through analysis of local and global mechanical properties through hardness and through lap shear tests, respectively, over time. A series of hardness maps are depicted in Figure 25. Two selected lines of measurements, on the middle of the top sheet for two conditions, are shown in Figure 26.

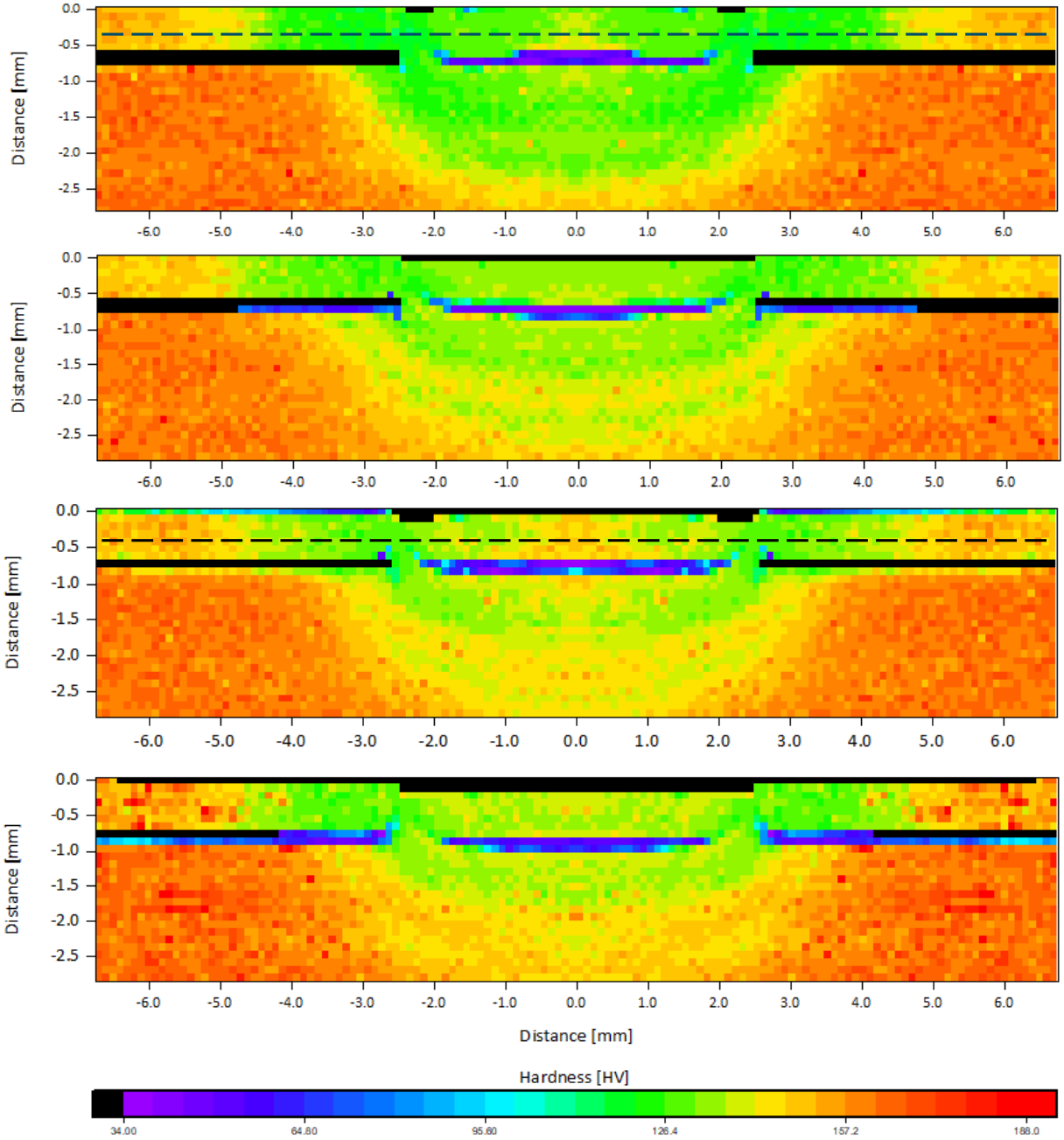

Figure 25 - Hardness Maps for samples after natural aging time. As-welded, 4 days, 7 days and 30 days are represented from top to bottom. Lines are highlighted in the middle of the thickness of the top sheet for two conditions.

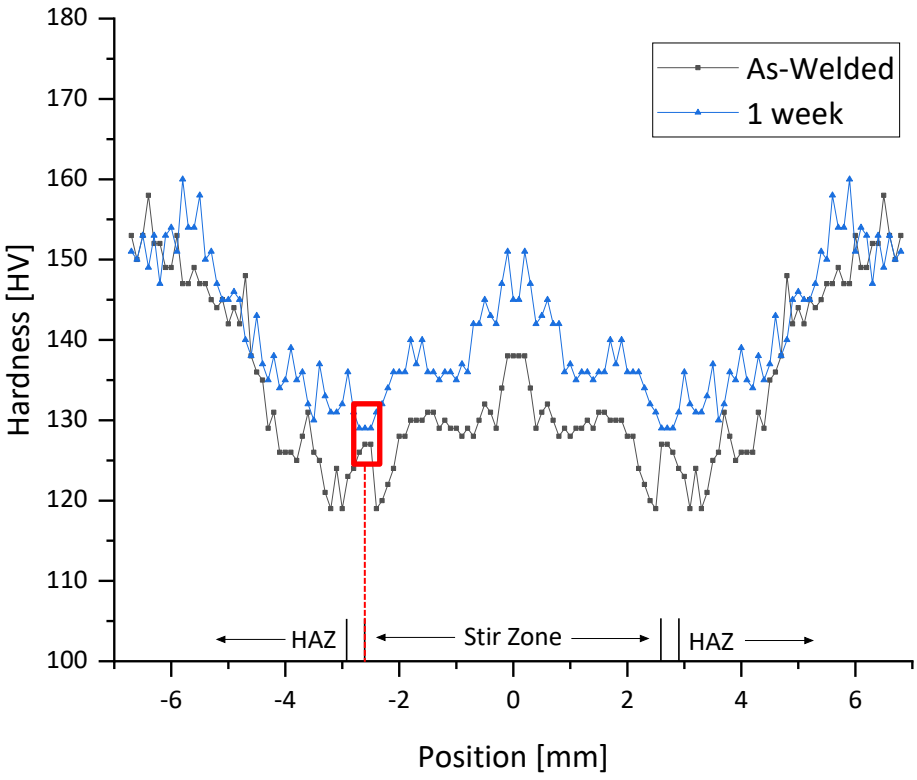

Figure 26 - Hardness lines from the regions highlighted in Figure 25. SZ/TMAZ interface highlighted by a square.

From Figure 25 it is possible to observe that some regions of the weld hardened over time, going from green tones to yellow and orange tones. This indicates that the temperatures reached in the process were high enough to dissolve precipitates and promote post-welding natural aging. It is also possible to observe that most of the hardening took place in the first 7 days after welding, and that no significant amount of aging occurs after this point.

The regions which hardened the most were the heat affected zone and stir zone. These regions experience the highest temperatures and naturally more precipitate dissolution. Thus, these are the regions with most potential for re-precipitation. The thermomechanically affected region is too small to be distinguished in the scale of the hardness map, prohibiting strong conclusions to be drawn about it.

When analyzing Lap Shear Strength, tests showed no significant variation of strength over time, as shown in Figure 27. This implies that natural aging affects hardness without affecting the overall mechanical performance of the weld.

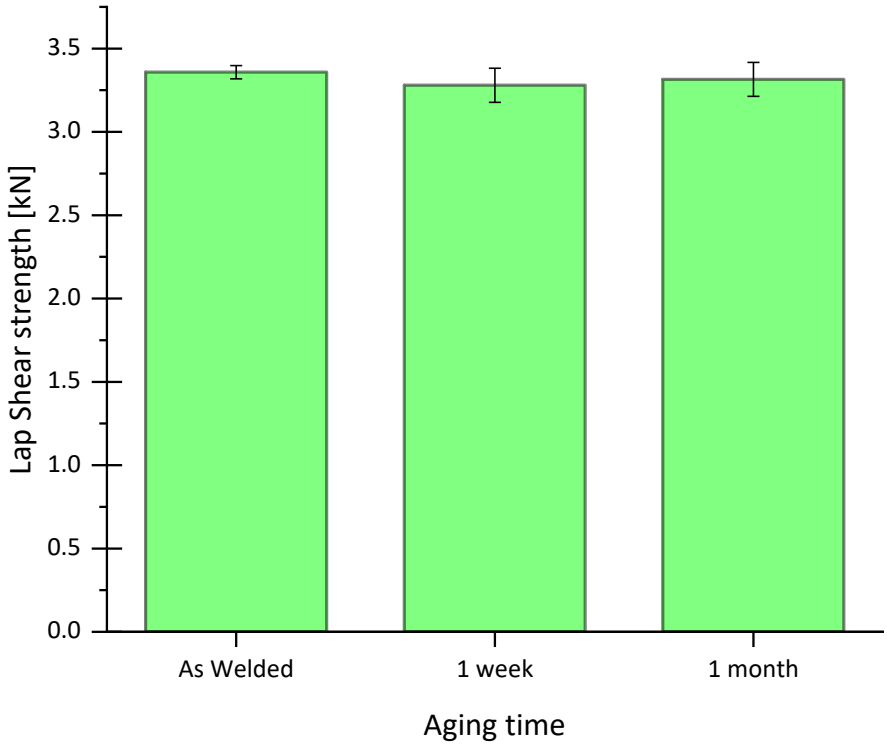

Figure 27 - Graph of the Lap Shear Tests performed to evaluate Natural Aging.

One possible theory as for why this may happen relates to the primary paths for crack propagation described in previous sections. The two main interfaces for failure are solute poor regions. Thus, these regions present a lower potential for precipitation and consequently for hardening. This is confirmed by Figure 26, in which the hardness points along the SZ/TMAZ interface are highlighted by a square. These points show almost no increase in hardness, which in turn implies that no additional resistance for crack propagation is present, and therefore, Lap Shear Strength remains relatively unchanged.

5.4 Tool Wear

To assess how tool wear progresses and how it influences weld performance, an analysis was made investigating the logical steps of this influence. Initially, the tool geometry was evaluated with the progression of wear. Then, the effects that the geometrical changes in the tool caused on the weld surface were observed. Lastly, the influence of these effects on Lap Shear Strength was measured and a causal relationship was established.

5.4.1 Evolution of wear effect on tool geometry

Initially, visual observation showed that wear is already present after 15 welds (Condition II) and it is clearly pronounced after 200 welds (Condition III), as shown in Figure 28. The number of welds performed show that wear effect is comparable to Montag et al. [49], who reported a high initial wear on the first 235 welds. This happened regardless of differences in the tool's dimensions, materials and design, as well as differences in process variables, such as Plunge Depth. Furthermore, the focal regions this wear, which can be visually identified in Figure 28, are also fairly consistent with what was reported by Montag et al [49], which state that the most worn and second most worn regions, in terms of deviation from the original dimensions, are the points 2 mm and 0 mm distant from the tip of the shoulder, identified in Figure 28 as regions (A) and (B) respectively.

This observation is also coherent with the explanation proposed by De Castro [50], who also reports a great level of tool wear on a region adjacent to the adjustable shoulder's tip. The proposed explanation states that with increasing welding cycles, plasticized aluminum adheres to the tool. After tool cool-down, this adhesive junction between Al and the tool material breaks off at the beginning of the following welding cycles, when the Al is not yet plasticized. This phenomenon causes the tip of the shoulder (Region A) to suffer from adhesive wear and decrease in diameter. Consequently, the gap between the outer surface of the shoulder and inner surface of the clamping ring increases. A

different explanation, however, is required to explain the wear at 2 mm from the tip of the shoulder (Region B), and it consists of three main factors.

After this increase in the gap between tool parts, plasticized material starts to more easily infiltrate and load this gap. According to Montag et al.[49] this increases the torque necessary to maintain the same rotation speed, thus increasing temperature, which is the first factor to contribute to wear in this region. The second factor is the elevated shear rates experienced by the outer edge of shoulder. The interface between probe and shoulder not only has a smaller radius (and consequently a smaller linear velocity), but also has both parts rotating at the same speed and in the same direction. On the other hand, the outer edge of the shoulder is rotating faster, and its clamping ring counterpart is stationary, increasing shear rates on the region. Finally, since the shoulder is manufactured of MP 159® and the clamping ring is made of standard HOTVAR®, different thermal expansion coefficients (14.3 μm/mºC for MP 159® [62] and 12.6μm/mºC for HOTVAR® [63]) increase the radial force the expanding shoulder exerts on the not-as-much expanding clamping ring.

Region B in Figure 28, 2-mm distant from the shoulder tip, is kept inside the clamping ring for all the welding cycle (given that the highest penetration depth was less than 1 mm) and thus has the most critical combination of temperature, shear rates and expansion-driven force. The distance between this worn region and the shoulder tip is approximately twice the Plunge Depth, which was also a fact for the worn regions described by De Castro [50].

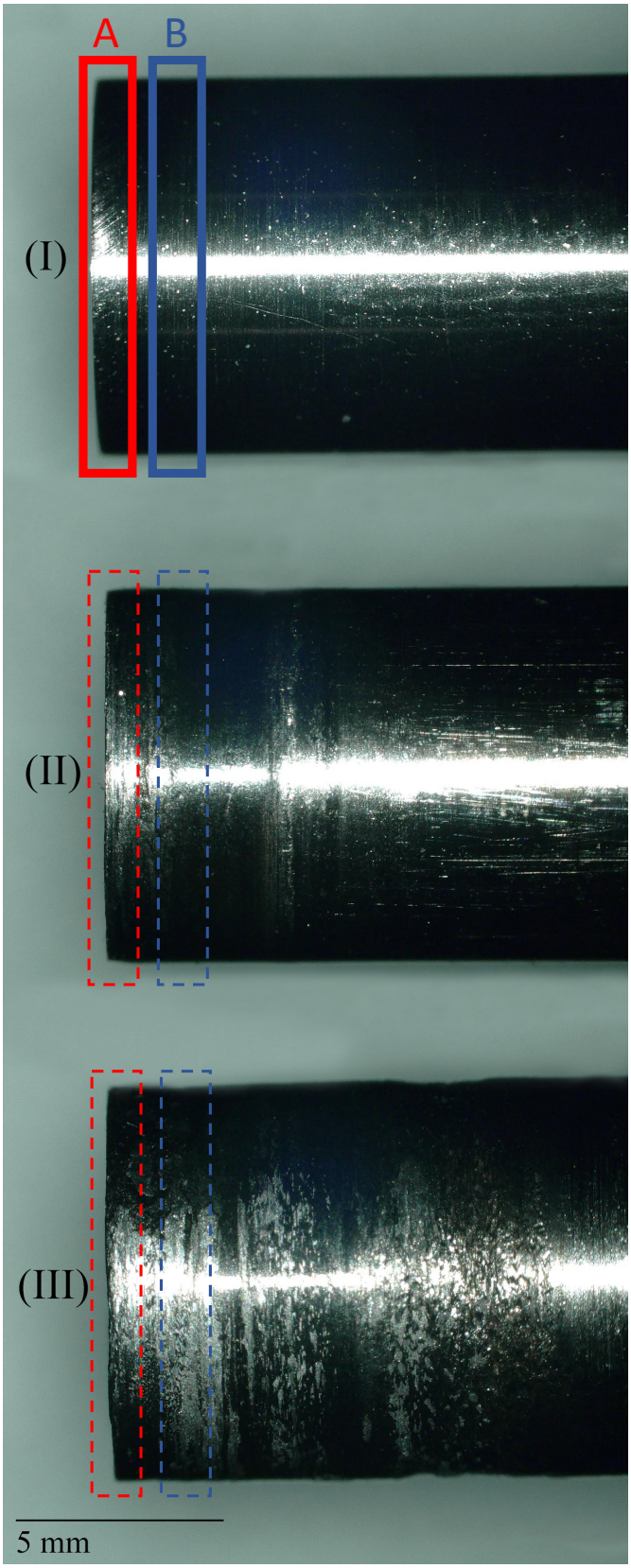

Figure 28 - Adjustable shoulder in different wear conditions where: (I) 0 welds performed, (II) 15 welds performed, (III) 200 welds performed.

Aside from radial decrease in the shoulder dimensions, a reduction in length on the inner surface of the shoulder was observed. Material displacement to the outer edge caused plastic deformation of this tool part, ultimately resulting in a protruding region on the outer edge of the shoulder tip. This feature is also reported by Montag et al [49]. In order to better evaluate the evolution of this protrusion, topography maps of this surface are shown in Figure 29. It can be observed that the protrusion clearly progresses with the increasing number of welds. In condition I, the tip of the shoulder is basically flat and, as wear evolves to conditions II and III, the outer edge increases in height, while the inner edge decreases.

Given that this surface of the tool is the first and last to be in contact with the sheets, alterations in geometry may affect the surface quality of the welds and ultimately, Lap Shear Strength.

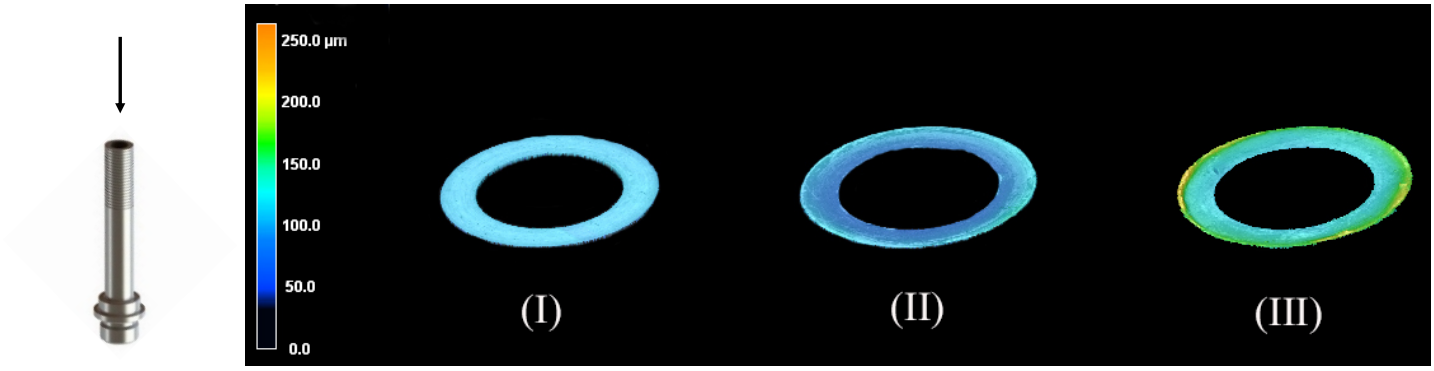

Figure 29 – Topography maps of the tip surface of the adjustable shoulder showing evolving plastic deformation where: (I) 0 welds performed, (II) 15 welds performed, (III) 200 welds performed.

5.4.2 Impact of worn-out tool on weld surface

The surface of a weld produced by the most worn tool condition studied (III) can be observed in Figure 30. It is evident that the aforementioned protruding deformation on the tip of the sleeve matches the outermost region of the weld (Figure 31), indicating that the wear can be associated with modifications of important geometric aspects of the welds.

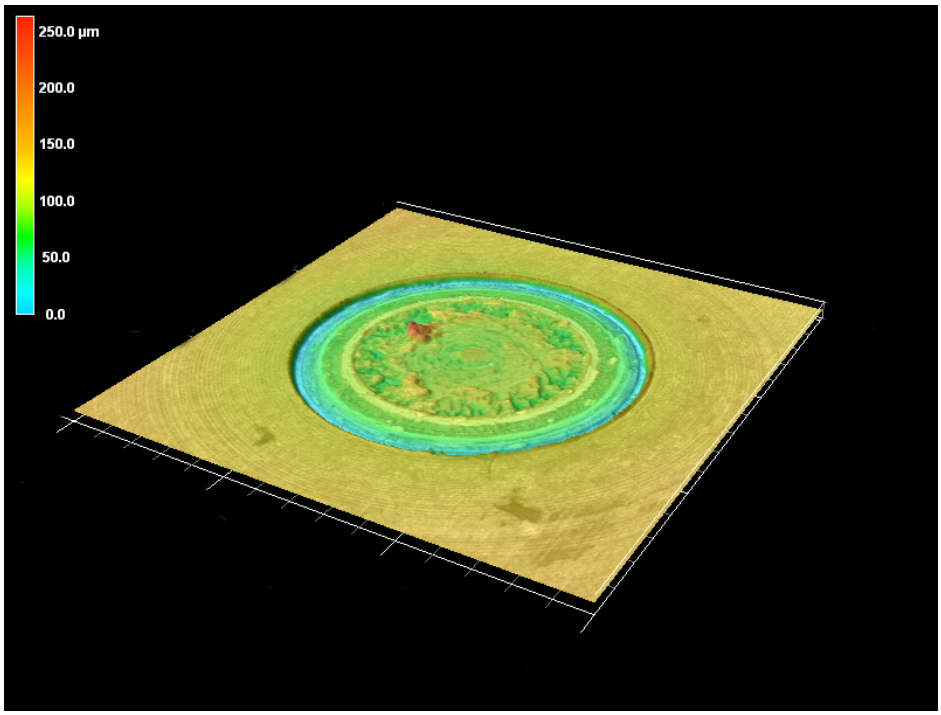

Figure 30 - Surface of a weld produced by the most worn tool condition (III).

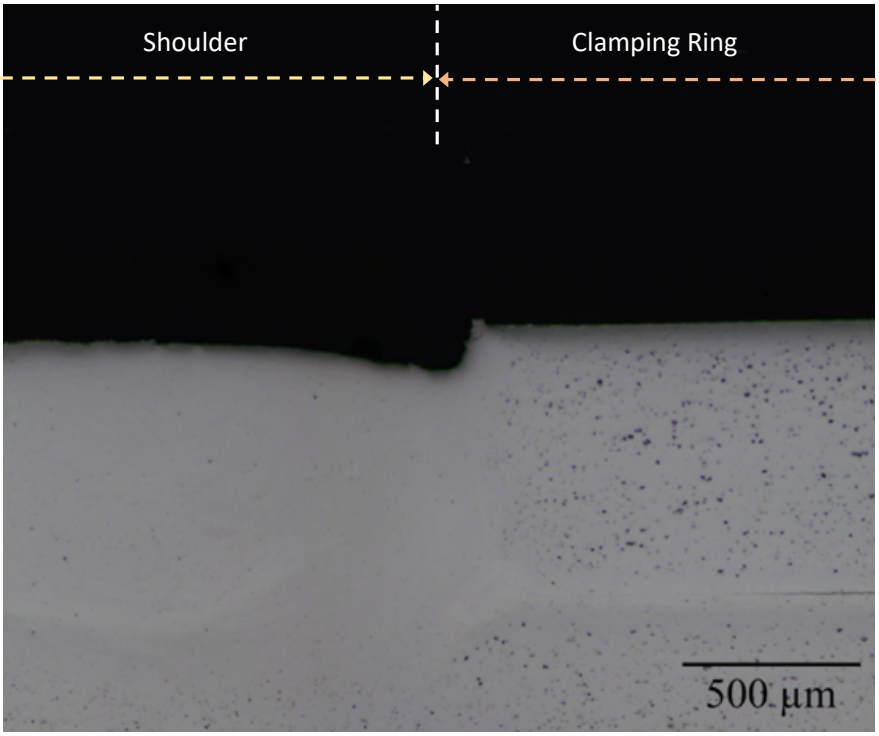

Figure 31 - Cross section of a weld produced by the most worn tool condition (III).

From a cross-sectional standpoint, the presence of this notch alters the geometry of the outer limits of the stir zone as shown in Figure 31. This ultimately

leads to a reduction in effective thickness of the top sheet in this position, which can lead to Lap Shear Strength reduction [36, 64].

5.4.3 Impact on Lap Shear Strength

The Lap Shear Strength was measured for welds produced by a new tool (condition I) and a tool after 200 welds (condition III). Since the alloy used is subject to natural aging after welding, tests were reproduced in three different aging times, aiming to guarantee that the effects observed were homogeneous and stable after aging was completed. Results shown in Figure 32 suggest that the wear effect significantly diminished weld Lap Shear Strength, regardless of the aging time the weld was subjected to.

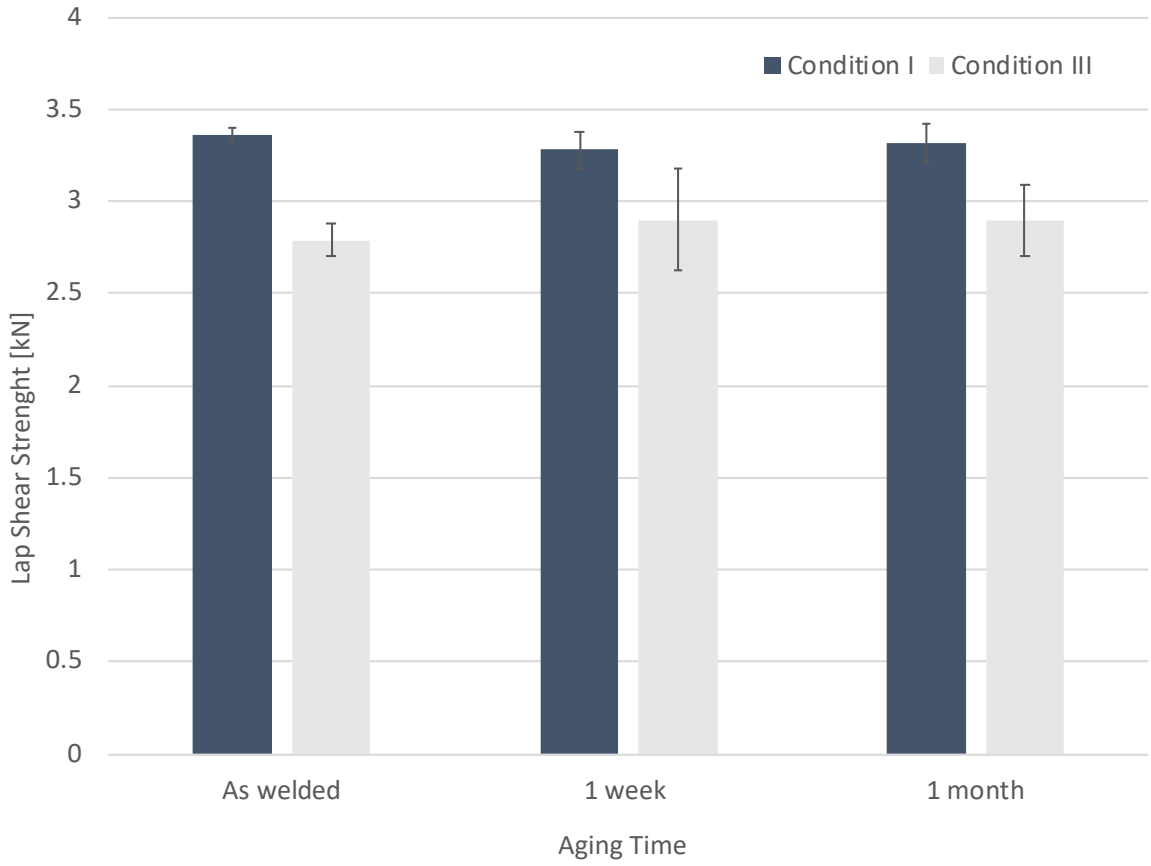

Figure 32 - Lap Shear Strength in different tool wear conditions, for multiple natural aging times.

Although this study contemplates only a comparison of extreme conditions in contrast to a series of measurements, this reduction in strength in relative terms is considerable when compared to other results in the literature. Montag et al [49] performed a series of measurements in intervals through 3,500 welding points and reported that no significant influence on Lap Shear Strength was observed. De Castro [50] also studied the variation of weld strength in a series of intervals through 2,350 cycles and observed different behaviors with wear progression. The first stage (weld 1 through 1,350) also presented a decrease in Lap Shear Strength. However, it took close to 1,000 welds to observe a decrease in the mean value of strength similar to the one observed in Figure 32 (ranging from 12 to 17%) which was reached after performing 200 welds.

This premature reduction in Lap Shear Strength can be explained by the sequence of causal events already presented. In order to provide the proper basis for the explanation, it is important to point out that all of the samples fractured in a pullout mode [4, 5], as shown by the cross-section in Figure 33. In this type of fracture, crack under static loading propagates through the partial bonding region of the hook and subsequently through the upper sheet, along the interface between stir zone and thermomechanically affected zone. Therefore, studies involving features such as the hook defect usually analyze the impact of this feature through the effective thickness of the top sheet [36, 64]. Analogously, the notch observed in this study also reduces this effective thickness, albeit from the surface instead of the interface between sheets.

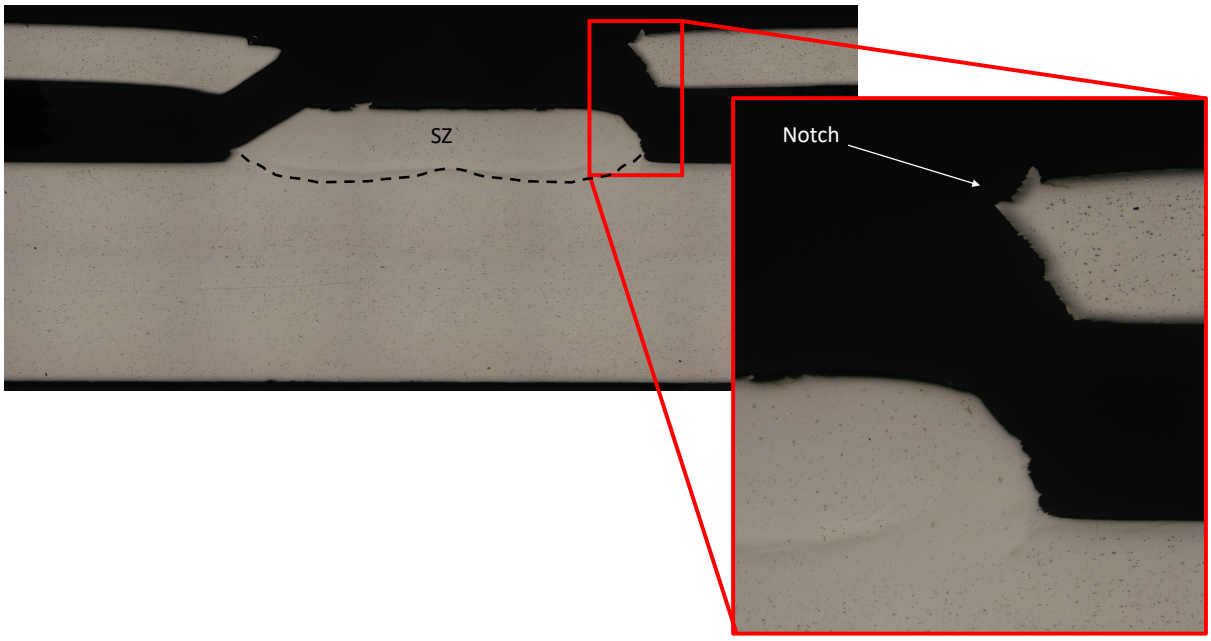

Figure 33 - Pullout fracture, in which the notch is highlighted atop the fracture path.

The size of the notch was measured using a Confocal Laser Microscope, and the percent decrease in effective thickness was calculated, given that the hook was flat in all cases. This percent decrease was compared to the percent decrease in Lap Shear Strength in Table 7. The similarity in the values observed confirm that notch size and reduction in strength are directly correlated.

Table 7 - Mean decrease in Lap Shear Strength and effective thickness between the maiden tool (Condition I) and worn-out tool (Condition II), for all ageing times

Mean Decrease	**As-welded**	**1 week**	**1 month**
Lap Shear Strength	17%	12%	13%
Effective Thickness	18%	12%	14%

In summary, as tool wear progresses, the geometry of the adjustable shoulder is deformed. This generates a protrusion in the outer edge of the shoulder. In turn, during the welding process, this protrusion translates to the formation of a notch on the surface of the spot welds. The larger the notch, the higher the reduction in effective thickness of that region. As the effective

thickness is reduced, so is the path for crack propagation. This leads to a decreased load-bearing area, and consequently failure at inferior loads.

6 CONCLUSIONS

This master's work performed a technical feasibility analysis and optimized the Refill Friction Stir Spot Welding process in 2A12 sheets of different thicknesses (0.8mm to 3.0mm) using a tool with reduced dimensions. Additionally, aspects of the metallurgical and mechanical behaviors of the welds, alongside the wear behavior of the tool were studied, and the following conclusions could be drawn:

1. Utilizing a tool with reduced dimensions did not affect the technical feasibility of the process, once a defect-free processing window was obtained and most welds surpassed usual aerospace requirements for mechanical properties.
2. The optimized welding parameters were 2380 rpm Rotational Speed, 1mm/s Plunge Speed and 0.95mm Plunge Depth. These parameters generate a condition with 3.2 ± 0.1kN Lap Shear Strength.
3. Plunge Depth significantly affects two microstructural geometrical features: Bonded Width and Layer Width. These features directly affect weld strength, especially when interfacial shear fracture is present. Consequently, Plunge Depth is the most significant variable to explain Lap Shear Strength variation as a function of process parameters.
4. Crack under static loading originates from the stress-concentrating hook and propagates through one of two paths with least resistance. Therefore, two main fracture modes present and the pullout mode is associated with the optimal condition.
5. Natural aging happens after processing and is mostly stable after 7 days. This process affects local mechanical properties, with observable hardening of a few weld regions. This, however, does not translate to global mechanical properties because preferable crack propagation paths present lower potential for precipitation.
6. A combination of adhesive wear and factors such as high temperature, high shear rates and the expansion coefficient of tool parts affect tool

geometry. This ultimately generates a protrusion on the outer edge of the adjustable shoulder's tip.

7. Welds produced by the worn-out tool presented significantly lower Lap Shear Strength. This effect can also be attributed to the changes in tool geometry. The protrusion formed on the tool translates to the formation of a notch on the outermost limits of the welding spot. This reduces the effective thickness of the top sheet, consequently decreasing Lap Shear Strength, regardless of the ageing time.

7 SUGGESTIONS FOR FUTURE WORK

This work aimed to provide a comprehensive view on the main aspects of the Refill FSSW process utilizing a tool with reduced dimensions. Additionally, it studied a novel sheets configuration, welding thin-to-thick sheets, comparative to current state of the art. In doing so, several areas were found to be deserving of further investigation and should be highlighted:

- Welding thicker sheets with a smaller tool - one of the reasons why the process was feasible with the reduced tool may be associated with the reduced dimension of the top sheet. Therefore, welding conventional thickness sheets (around 2mm) with a smaller tool should provide an interesting comparison with the standard tool in terms of strength/area and strength/energy ratios.

- Systematic investigation of tool materials – although this study provided preliminary insight on how tool wear progresses, its conclusions are limited to the specific tool used in this project. Studies with the primary focus on varying tool materials and investigating the influence on tool wear and weld performance should be conducted.

- Systematic investigation of tool design – Analogously to the previous suggestion, a study should be made with focus on tool design. A wide variety of designs can be found in the literature, and no particular explanation as for why they are used. A better understanding of how this influences the process, along with an optimized design should significantly enhance results in all the fields of study.

8 REFERENCES

1. Da Silva AAM, Dos Santos JF, Rosendo TR, et al (2007) Performance evaluation of 2-mm thick alclad AA2024 T3 aluminium alloy friction spot welding. SAE Tech Pap. https://doi.org/10.4271/2007-01-3812

2. Tier M, Rosendo T, Olea CW, et al (2008) The Influence of Weld Microstructure on Mechanical Properties of Alclad AA2024-T3 Friction Spot Welded. 7th Int Symp Frict Stir Weld 20–22

3. Suhuddin U, Campanelli L, Bissolatti M, et al (2013) A review on microstructural and mechanical properties of friction spot welds in Al-based similar and dissimilar joints. Proc 1st Int Jt Symp Join Weld 15–21. https://doi.org/10.1533/978-1-78242-164-1.15

4. Amancio-Filho ST, Camillo APC, Bergmann L, et al (2011) Preliminary Investigation of the Microstructure and Mechanical Behaviour of 2024 Aluminium Alloy Friction Spot Welds. Mater Trans 52:985–991. https://doi.org/10.2320/matertrans.L-MZ201126

5. Campanelli LC, Suhuddin UFH, Antonialli AÍS, et al (2013) Metallurgy and mechanical performance of AZ31 magnesium alloy friction spot welds. J Mater Process Technol 213:515–521. https://doi.org/10.1016/j.jmatprotec.2012.11.002

6. Li Z, Gao S, Ji S, et al (2016) Effect of Rotational Speed on Microstructure and Mechanical Properties of Refill Friction Stir Spot Welded 2024 Al Alloy. J Mater Eng Perform 25:1673–1682. https://doi.org/10.1007/s11665-016-1999-2

7. Shen J, Suhuddin UFH, Cardillo MEB, Dos Santos JF (2014) Eutectic structures in friction spot welding joint of aluminum alloy to copper. Appl Phys Lett 104:2014–2017. https://doi.org/10.1063/1.4876238

8. Suhuddin U, Fischer V, dos Santos J (2013) Formation of Intermetallic Compounds in Dissimilar Friction Spot Weld of Al to Mg Alloys. Mater Sci Forum 765:731–735. https://doi.org/10.4028/www.scientific.net/MSF.765.731

9. Plaine AH, Suhuddin UFH, Afonso CRM, et al (2016) Interface formation and properties of friction spot welded joints of AA5754 and Ti6Al4V alloys. Mater Des 93:224–231. https://doi.org/10.1016/j.matdes.2015.12.170

10. Zhu L, Li N, Childs PRN (2018) Light-weighting in aerospace component and system design. 7:103–119. https://doi.org/10.1016/j.jppr.2018.04.001

11. Braga DFO, Tavares SMO, Da Silva LFM, et al (2014) Advanced design for lightweight structures: Review and prospects. Prog Aerosp Sci 69:29–39. https://doi.org/10.1016/j.paerosci.2014.03.003

12. Dursun T, Soutis C (2014) Recent developments in advanced aircraft aluminium alloys. Mater Des 56:862–871. https://doi.org/10.1016/j.matdes.2013.12.002

13. Adams JH, Ammons M, Avery H, Barnhurst R (1992) ASM Metals HandBook - Properties and Selection: Nonferrous Alloys and Special-Purpose Materials

14. Vasudevan AK, Doherty RD (1989) Aluminum Alloys - Contemporary Research and Applications

15. Starke EA, Staley JT (1996) Application of modern aluminum alloys to aircraft. Prog Aerosp Sci 32:131–172. https://doi.org/10.1016/0376-0421(95)00004-6

16. Immarigeon JP, Holt RT, Koul AK, et al (1995) Lightweight materials for aircraft applications. Mater Charact 35:41–67. https://doi.org/10.1016/1044-5803(95)00066-6

17. Zhang X, Chen Y, Hu J (2018) Recent advances in the development of aerospace materials. Prog Aerosp Sci 97:35–60. https://doi.org/10.1016/j.paerosci.2018.01.001

18. Mishra RS, Sidhar H (2017) Physical Metallurgy of 2XXX Aluminum Alloys. In: Friction Stir Welding of 2XXX Aluminum Alloys Including Al-Li Alloys. pp 15–36

19. Wang SC, Starink MJ (2005) Precipitates and intermetallic phases in precipitation hardening Al–Cu–Mg–(Li) based alloys. Int Mater Rev 50:193–215. https://doi.org/10.1179/174328005X14357

20. Wang SC, Starink MJ (2007) Two types of S phase precipitates in Al-Cu-Mg alloys. Acta Mater 55:933–941. https://doi.org/10.1016/j.actamat.2006.09.015

21. Tier MD, Rosendo TS, Dos Santos JF, et al (2013) The influence of refill FSSW parameters on the microstructure and shear strength of 5042 aluminium welds. J Mater Process Technol 213:997–1005. https://doi.org/10.1016/j.jmatprotec.2012.12.009

22. Iwashita T. Method and apparatus for joining. Mazda Motor Corporation: US 6601751 B2. Depósito: 19/04/2001. Concessão: 05/08/2003.

23. Schilling C., dos Santos J. Method and device for joining at least two adjoiningwork pieces by friction welding. GKSS Forschungszentrum Geesthacht GmbH: US 6722556 B2. Depósito: 16/05/2002. Concessão: 20/04/2004.

24. de Castro CC, Plaine AH, Dias GP, et al (2018) Investigation of geometrical features on mechanical properties of AA2198 refill friction stir spot welds. J Manuf Process 36:330–339. https://doi.org/10.1016/j.jmapro.2018.10.027

25. Pieta G, Dos Santos J, Strohaecker TR, Clarke T (2014) Optimization of friction spot welding process parameters for AA2198-T8 sheets. Mater Manuf Process 29:934–940. https://doi.org/10.1080/10426914.2013.811727

26. Brzostek RC, Suhuddin U, dos Santos JF (2017) Fatigue assessment of refill friction stir spot weld in AA 2024-T3 similar joints. Fatigue Fract Eng Mater Struct 1–16. https://doi.org/10.1111/ffe.12764

27. de Barros PAF, Campanelli LC, Alcântara NG, Dos Santos JF (2017) An investigation on friction spot welding of AA2198-T8 thin sheets. Fatigue Fract Eng Mater Struct 40:535–542. https://doi.org/10.1111/ffe.12512

28. Reimann M, Goebel J, Gartner TM, Jorge F (2017) Refilling termination hole in AA 2198 – T851 by refill friction stir spot welding. J Mater Process Tech 245:157–166. https://doi.org/10.1016/j.jmatprotec.2017.02.025

29. Ji S, Wang Y, Zhang J, Li Z (2017) Influence of rotating speed on microstructure and peel strength of friction spot welded 2024-T4 aluminum alloy. Int J Adv Manuf Technol 90:717–723. https://doi.org/10.1007/s00170-016-9398-2

30. Rosendo T, Parra B, Tier MAD, et al (2011) Mechanical and microstructural investigation of friction spot welded AA6181-T4 aluminium alloy. Mater Des 32:1094–1100. https://doi.org/10.1016/j.matdes.2010.11.017

31. Reimann M, Gartner T, Suhuddin U, et al (2016) Keyhole closure using friction spot welding in aluminum alloy 6061-T6. J Mater Process Technol 237:12–18. https://doi.org/10.1016/j.jmatprotec.2016.05.013

32. Reimann M, Goebel J, dos Santos JF (2017) Microstructure and mechanical properties of keyhole repair welds in AA 7075-T651 using refill friction stir spot welding. Mater Des 132:283–294. https://doi.org/10.1016/j.matdes.2017.07.013

33. Kubit A, Kluz R, Trzepieciński T, et al (2018) Analysis of the mechanical properties and of micrographs of refill friction stir spot welded 7075-T6 aluminium sheets. Arch Civ Mech Eng 18:235–244. https://doi.org/10.1016/j.acme.2017.07.005

34. Effertz PS, Quintino L, Infante V (2017) The optimization of process parameters for friction spot welded 7050-T76 aluminium alloy using a Taguchi orthogonal array. Int J Adv Manuf Technol 91:3683–3695. https://doi.org/10.1007/s00170-017-0048-0

35. Effertz PS, Infante V, Quintino L, et al (2016) Fatigue life assessment of friction spot welded 7050-T76 aluminium alloy using Weibull distribution. Int J Fatigue 87:381–390. https://doi.org/10.1016/j.ijfatigue.2016.02.030

36. Santana LM, Suhuddin UFH, Ölscher MH, et al (2017) Process optimization and microstructure analysis in refill friction stir spot welding of

3-mm-thick Al-Mg-Si aluminum alloy. Int J Adv Manuf Technol 92:4213–4220. https://doi.org/10.1007/s00170-017-0432-9

37. Shen J, Lage SBM, Suhuddin UFH, et al (2017) Texture Development and Material Flow Behavior During Refill Friction Stir Spot Welding of AlMgSc. Metall Mater Trans A 49:241–254. https://doi.org/10.1007/s11661-017-4381-6

38. Suhuddin UFH, Fischer V, Dos Santos JF (2013) The thermal cycle during the dissimilar friction spot welding of aluminum and magnesium alloy. Scr Mater 68:87–90. https://doi.org/10.1016/j.scriptamat.2012.09.008

39. Suhuddin U, Fischer V, Kroeff F, dos Santos JF (2014) Microstructure and mechanical properties of friction spot welds of dissimilar AA5754 Al and AZ31 Mg alloys. Mater Sci Eng A 590:384–389. https://doi.org/10.1016/j.msea.2013.10.057

40. Shen J, Cardillo M, dos Santos JF (2014) A preliminary study on FSpW of dissimilar metal joints of Cu and Al. 10th Int Symp Frict Stir Weld

41. Plaine AH, Gonzalez AR, Suhuddin UFH, et al (2015) The optimization of friction spot welding process parameters in AA6181-T4 and Ti6Al4V dissimilar joints. Mater Des 83:36–41. https://doi.org/10.1016/j.matdes.2015.05.082

42. Plaine AH, Suhuddin UFH, Alcântara NG, dos Santos JF (2016) Fatigue behavior of friction spot welds in lap shear specimens of AA5754 and Ti6Al4V alloys. Int J Fatigue 91:149–157. https://doi.org/10.1016/j.ijfatigue.2016.06.005

43. André NM, Goushegir SM, Dos Santos JF, et al (2016) Friction Spot Joining of aluminum alloy 2024-T3 and carbon-fiber-reinforced poly(phenylene sulfide) laminate with additional PPS film interlayer: Microstructure, mechanical strength and failure mechanisms. Compos Part B Eng 94:197–208. https://doi.org/10.1016/j.compositesb.2016.03.011

44. André NM, Goushegir SM, dos Santos JF, et al (2018) Influence of the interlayer film thickness on the mechanical performance of AA2024-T3/CF-PPS hybrid joints produced by friction spot joining. Weld Int 32:1–10. https://doi.org/10.1080/09507116.2017.1347319

45. Vacchi GS, Plaine AH, Silva R, et al (2017) Effect of friction spot welding (FSpW) on the surface corrosion behavior of overlapping AA6181-T4/Ti-6Al-4V joints. Mater Des 131:127–134. https://doi.org/10.1016/j.matdes.2017.06.005

46. American Welding Society (2013) AWS D17.2 - Specification for Resistance Welding for Aerospace Applications

47. Shen Z, Ding Y, Gopkalo O, et al (2018) Effects of tool design on the microstructure and mechanical properties of refill friction stir spot welding

of dissimilar Al alloys. J Mater Process Technol 252:751–759. https://doi.org/10.1016/j.jmatprotec.2017.10.034

48. Nasiri AM, Shen Z, Hou JSC, Gerlich AP (2018) Failure analysis of tool used in refill friction stir spot welding of Al 2099 alloy. Eng Fail Anal 84:25–33. https://doi.org/10.1016/j.engfailanal.2017.09.009

49. Montag T, Wulfsberg JP, Hameister H, Marschner R (2014) Influence of tool wear on quality criteria for refill friction stir spot welding (RFSSW) process. Procedia CIRP 24:108–113. https://doi.org/10.1016/j.procir.2014.08.015

50. de Castro C.C. (2019) Refill Friction Stir Spot Welding: Evaluation of the Welding of AA2198-T8 Sheets and Preliminary Tool Wear Investigation. 121p. Masters Dissertation. Federal University of São Carlos.

51. Cavazzuti M (2013) Optimization methods: From theory to design scientific and technological aspects in mechanics. In: Optimization Methods: From Theory to Design Scientific and Technological Aspects in Mechanics. pp 13–41

52. Roy R.K. (2016) A Primer on the Taguchi method. 2nd Edition. Michigan USA: Society of Manufacturing Engineers.

53. Montgomery DC (2013) Design and Analysis of Experiments. 8th Edition. Arizona USA: John Wiley and Sons, Inc.

54. Ferreira SLC, Bruns RE, Ferreira HS, et al (2007) Box-Behnken design: An alternative for the optimization of analytical methods. Anal Chim Acta 597:179–186. https://doi.org/10.1016/j.aca.2007.07.011

55. Sahoo BK, Chakraborty U, Mukherjee J, Pal TK (2010) Optimization and Validation of Modulated Release Formulation of Ranitidine HCl by Response Surface Methodology. J Biomed Sci Res 2:76–85

56. Sathyamoorthy N, Magharla D, Chintamaneni P, Vankayalu S (2017) Optimization of paclitaxel loaded poly (ε-caprolactone) nanoparticles using Box Behnken design. Beni-Suef Univ J Basic Appl Sci 6:362–373. https://doi.org/10.1016/j.bjbas.2017.06.002

57. Yu XL, He Y (2017) Application of Box-Behnken designs in parameters optimization of differential pulse anodic stripping voltammetry for lead(II) determination in two electrolytes. Sci Rep 7:1–8. https://doi.org/10.1038/s41598-017-03030-2

58. International A (2013) ASTM D3162: Standard Test Method for Strength Properties of Adhesively Bonded Plastic Lap-Shear Sandwich Joints in Shear by Tension Loading. ASTM B Stand 03:2011–2014. https://doi.org/10.1520/D3164-03R11.2

59. International A (2017) ASTM E384-17: Standard Test Method for

Microindentation Hardness of Materials. ASTM B Stand 1–40. https://doi.org/10.1520/E0384-17

60. International A (2018) ASTM E92-17: Standard Test Methods for Vickers Hardness and Knoop Hardness of Metallic. 1–27. https://doi.org/10.1520/E0092-17.2

61. Li Z, Ji S, Ma Y, et al (2016) Fracture mechanism of refill friction stir spot-welded 2024-T4 aluminum alloy. Int J Adv Manuf Technol 86:1925–1932. https://doi.org/10.1007/s00170-015-8276-7

62. AZoM (2012) Super Alloy MP 159 ™ - Material Sheet. 3p.

63. UddeHolme (2011) HOTVAR - Material Sheet. 12p.

64. Badarinarayan H, Shi Y, Li X, Okamoto K (2009) Effect of tool geometry on hook formation and static strength of friction stir spot welded aluminum 5754-O sheets. Int J Mach Tools Manuf 49:814–823. https://doi.org/10.1016/j.ijmachtools.2009.06.001

APPENDIX A

The first approach of using the full-quadratic model, standard for the Box-Behnken design, lead to the ANOVA presented in Figure 34. This was not considered satisfactory due to the difference between R^2 and Adjusted R^2, explained in the results section, aside from a few features observable in the table. These include the p-value for the model, which was higher than 0,05, indicating a statistical 89% chance of the model being significant, and the extremely low value for the percentage contribution of the interaction between Plunge Depth and Rotational Speed (more than two hundred times lower than the second lowest value).

In order to improve on that, a backward elimination of terms was conducted. Afterwards, a manual elimination on the best-case scenario gave the outcome presented in the results section.

Analysis of Variance

Source	DF	Seq SS	Contribution	Adj SS	Adj MS	F-Value	P-Value
Model	9	2352414	85,01%	2352414	261379	3,15	0,110
Linear	3	1121655	40,53%	1121655	373885	4,51	0,069
Plunge Depth	1	838525	30,30%	838525	838525	10,11	0,025
Plunge Rate	1	114364	4,13%	114364	114364	1,38	0,293
Rotational Speed	1	168766	6,10%	168766	168766	2,03	0,213
Square	3	737947	26,67%	737947	245982	2,97	0,136
Plunge Depth*Plunge Depth	1	457976	16,55%	528586	528586	6,37	0,053
Plunge Rate*Plunge Rate	1	68806	2,49%	88137	88137	1,06	0,350
Rotational Speed*Rotational Speed	1	211166	7,63%	211166	211166	2,55	0,171
2-Way Interaction	3	492811	17,81%	492811	164270	1,98	0,235
Plunge Depth*Plunge Rate	1	285621	10,32%	285621	285621	3,44	0,123
Plunge Depth*Rotational Speed	1	275	0,01%	275	275	0,00	0,956
Plunge Rate*Rotational Speed	1	206916	7,48%	206916	206916	2,49	0,175
Error	5	414727	14,99%	414727	82945		
Lack-of-Fit	3	382209	13,81%	382209	127403	7,84	0,115
Pure Error	2	32519	1,18%	32519	16259		
Total	14	2767141	100,00%				

Model Summary

S	R-sq	R-sq(adj)	PRESS	R-sq(pred)
288,003	85,01%	58,03%	6188506	0,00%

Figure 34 - ANOVA for the full quadratic model

APPENDIX B

The adequacy checking of the model consisted of plotting the Normal Probability Plot for residuals, presented in Figure 35, as well as the residuals against fitted responses, order and each process parameter, shown in Figure 36 and Figure 37.

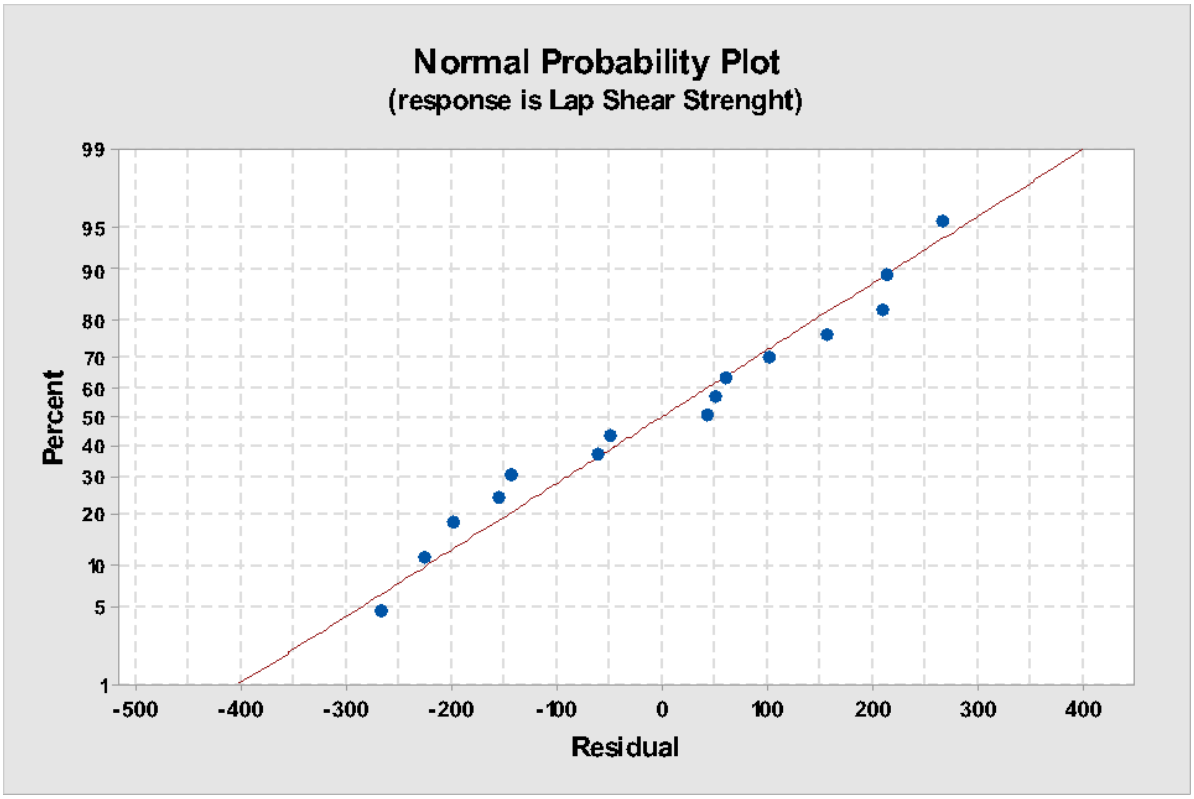

Figure 35 - Normal Probability Plot of residuals

The plots show normal distribution of the residuals, as well as completely random distribution with order and fitted value, indicating no tendency on the model. The standard residuals were also observed and found to be in the normal range of -3 to +3, with the highest residuals having absolute values of 2.

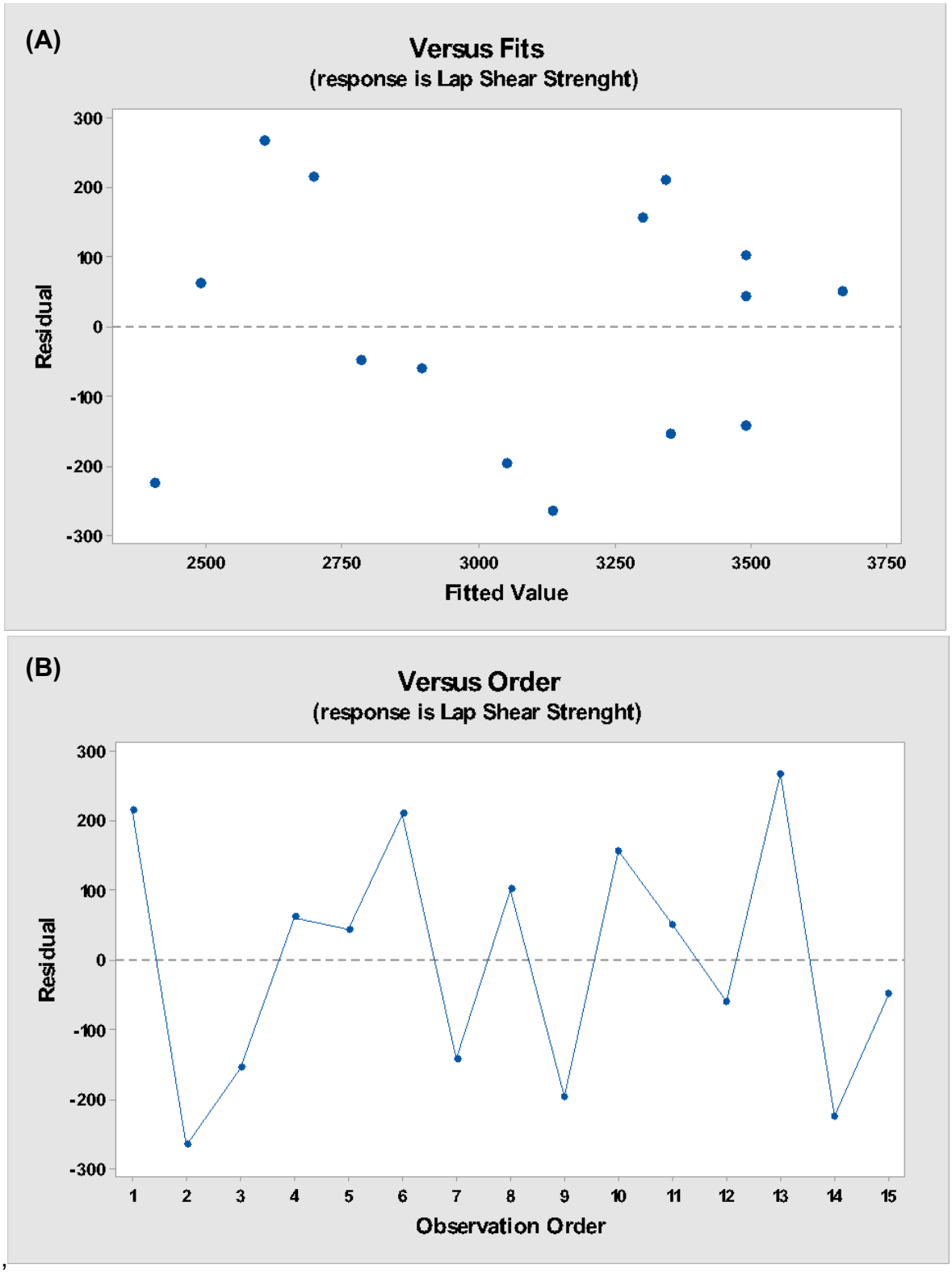

Figure 36 - Residuals plotted against (A) Fitted Value and (B) Observation Order.

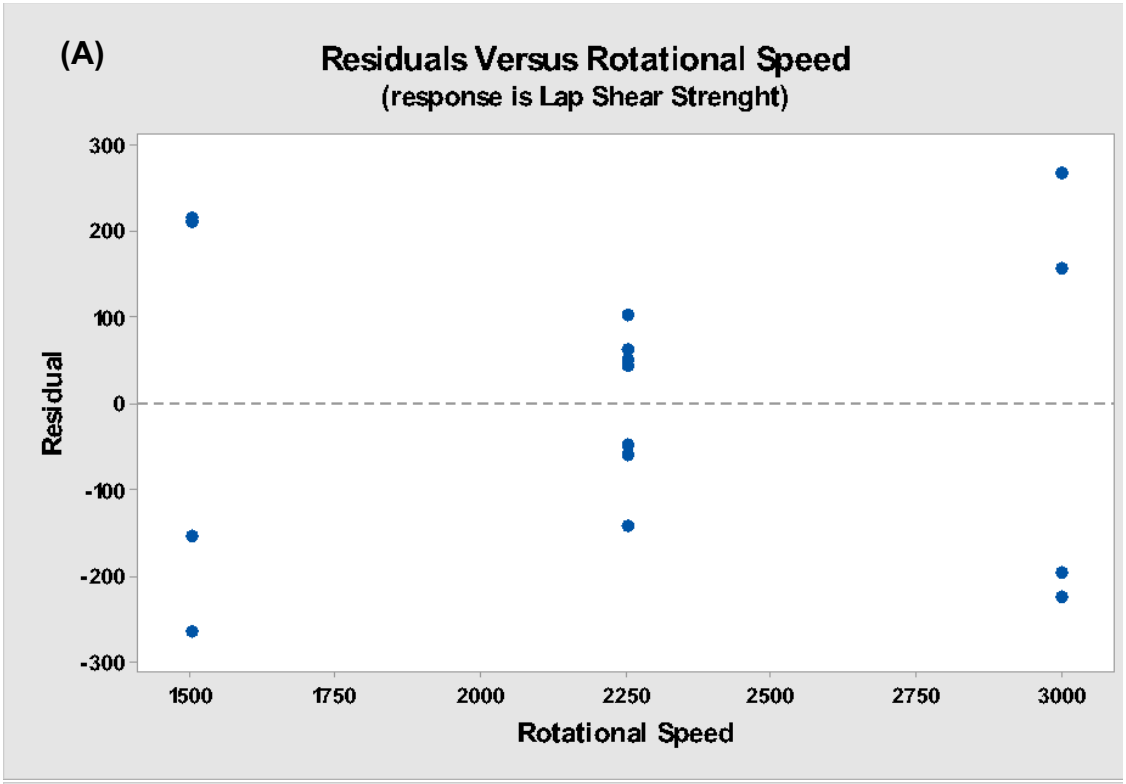
(A)
Residuals Versus Rotational Speed
(response is Lap Shear Strenght)
Residual
300
200
100
0
-100
-200
-300
1500
1750
2000
2250
2500
2750
3000
Rotational Speed

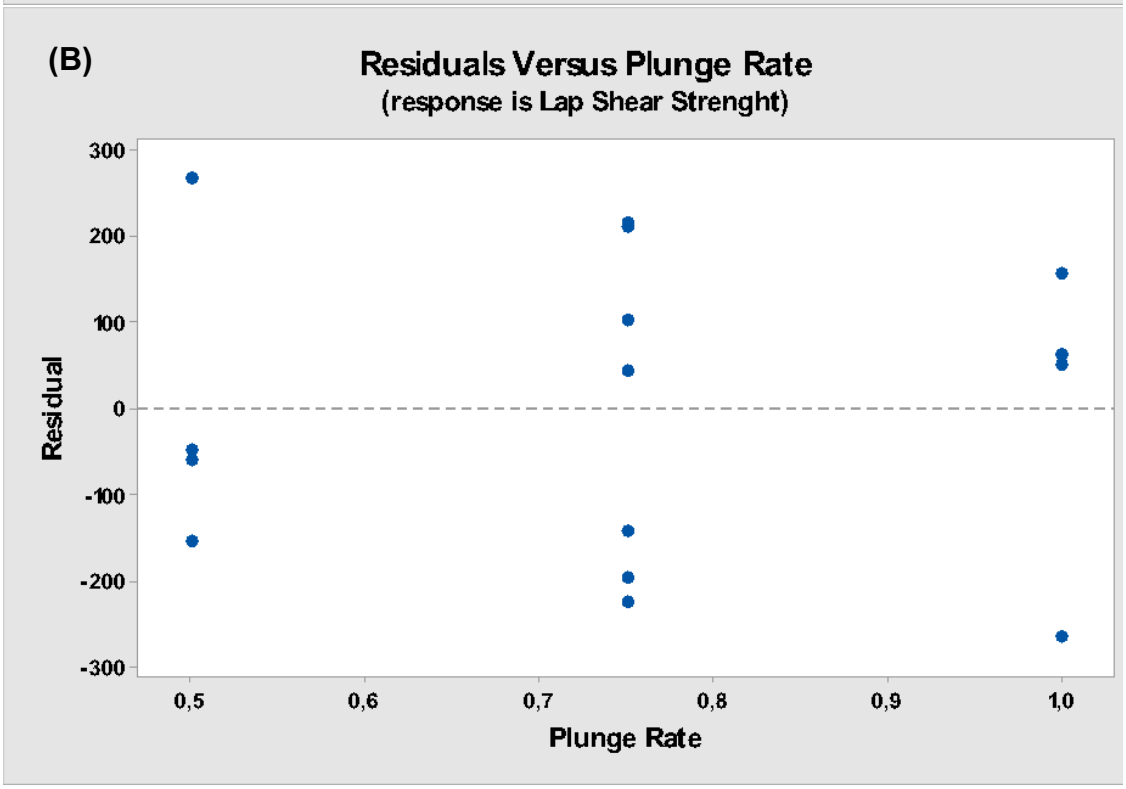
(B)
Residuals Versus Plunge Rate
(response is Lap Shear Strenght)
Residual
300
200
100
0
-100
-200
-300
0,5
0,6
0,7
0,8
0,9
1,0
Plunge Rate

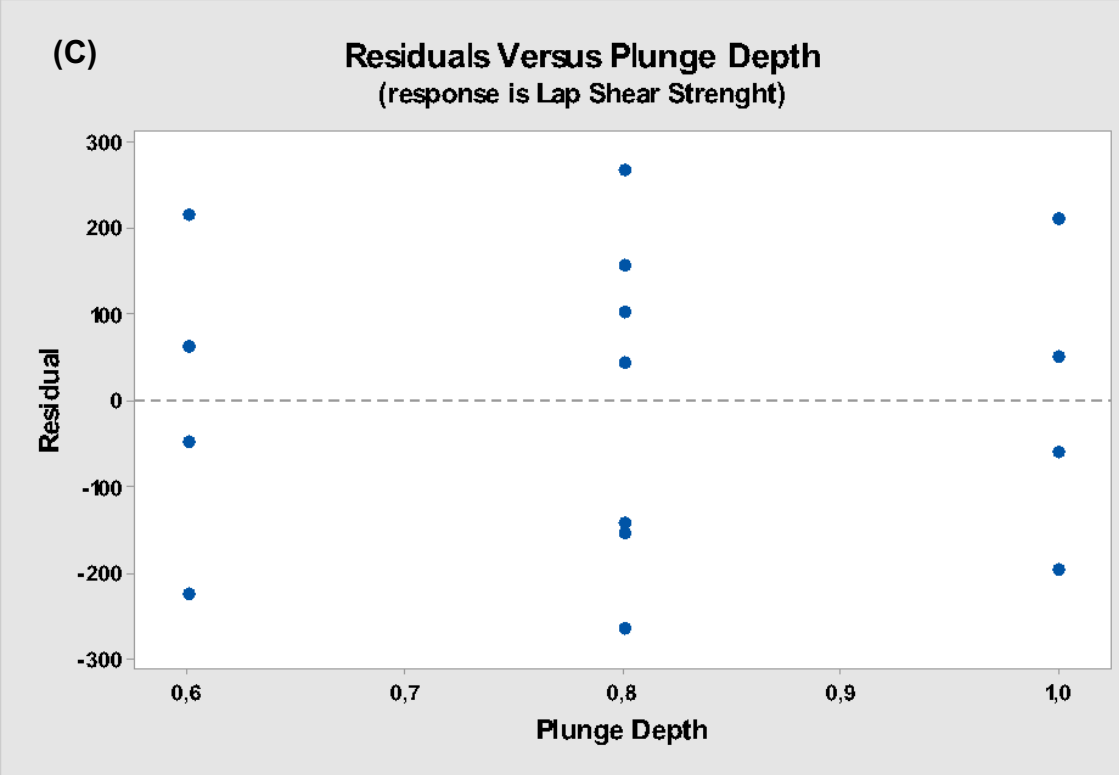

Figure 37 - Residuals plotted against variables (A) Rotational Speed, (B) Plunge Rate, (C) Plunge Depth.

These plots show a mild tendency of lower residual values when increasing Plunge Rate, as well as a slight tendency to have a lower variance for intermediate values of Rotational Speed. None of these tendencies, however, is sharp enough to cause concern.

Thus, the model was considered to fit the assumptions for the ANOVA, making it an adequate model to proceed the analysis with.

APPENDIX C

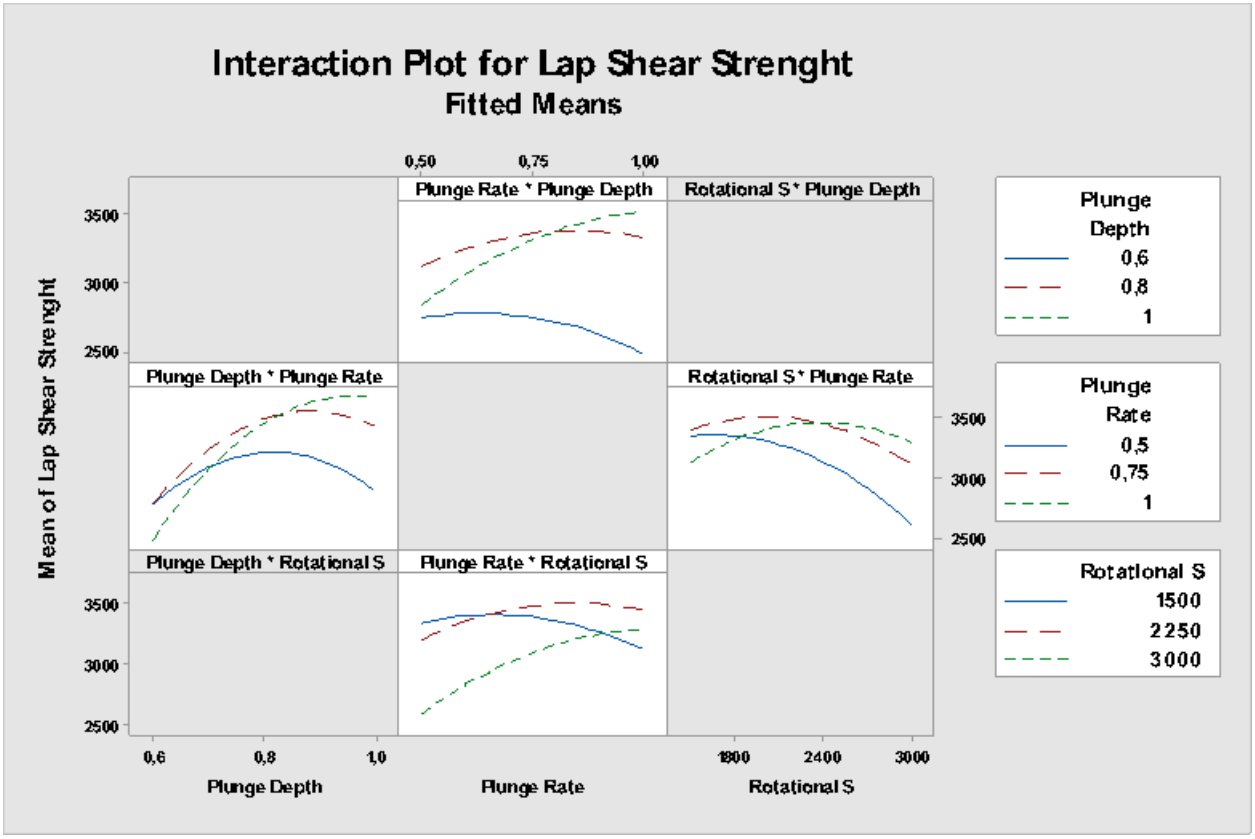

Figure 38 - Interaction Plots for the Box-Behnken model.

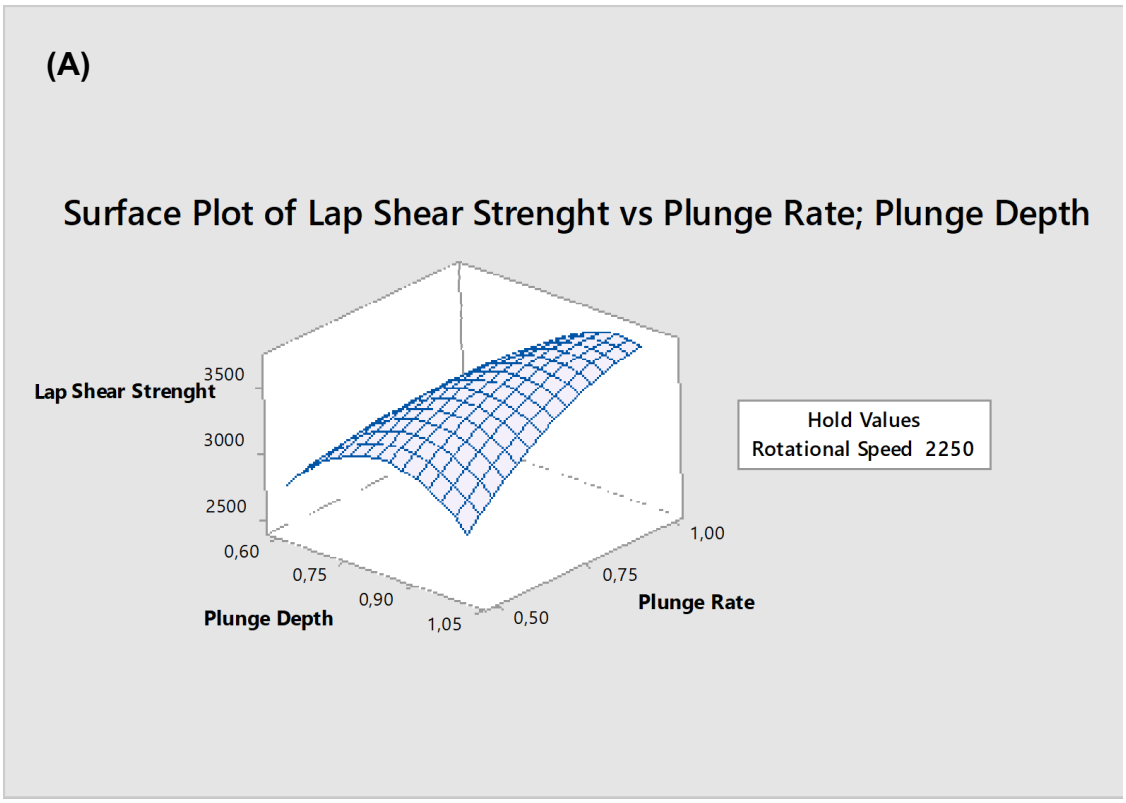

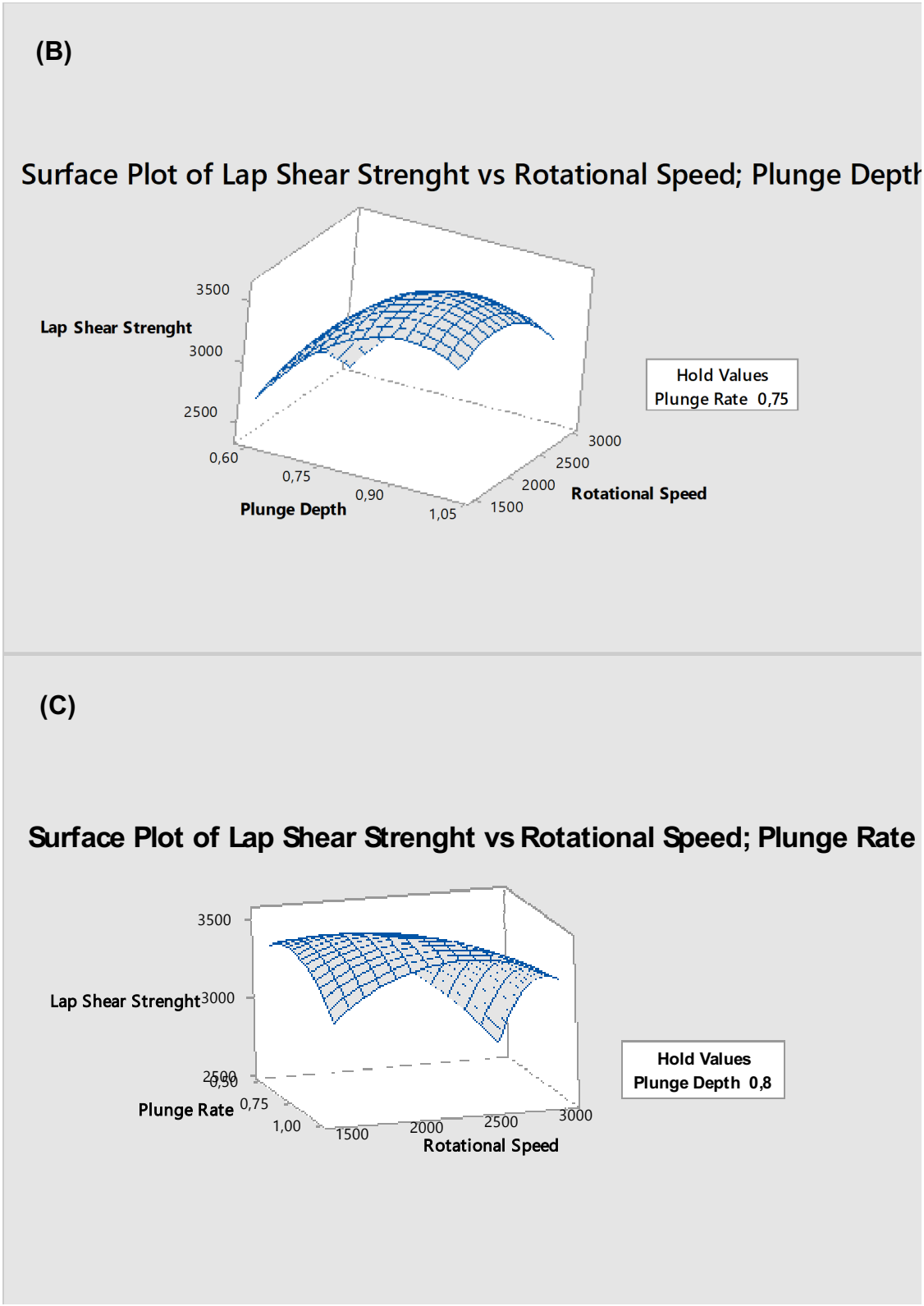

Figure 39 - Surface plots for Equation 3.

APPENDIX D

The Lap Shear Strength of the samples used in the Box-Behnken Design was plotted in crescent order, and the different modes of fracture were highlighted. It is possible to see from Figure 40 that the pullout mode cannot be associated with high or low values of strength. Given that it happened for intermediate strengths, it is likely related to other factors of the process.

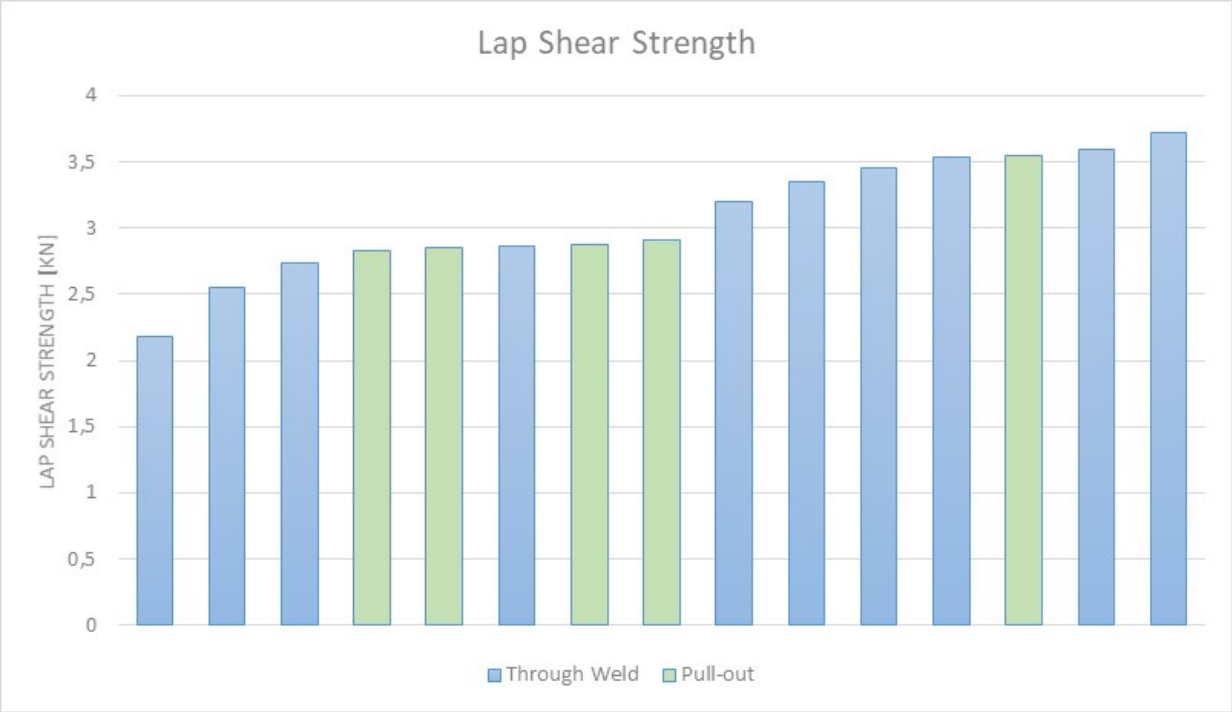

Figure 40 - Ascending Lap Shear Strength with two failure modes.

The strength was also plotted against the three parameters varied in the DoE, and again different modes of fracture were highlighted. These graphs are shown in Figure 41. Again, it is possible to observe both fracture modes in all values for all the parameters. Thus, it is impossible to establish any relationship between parameters and failure mode.

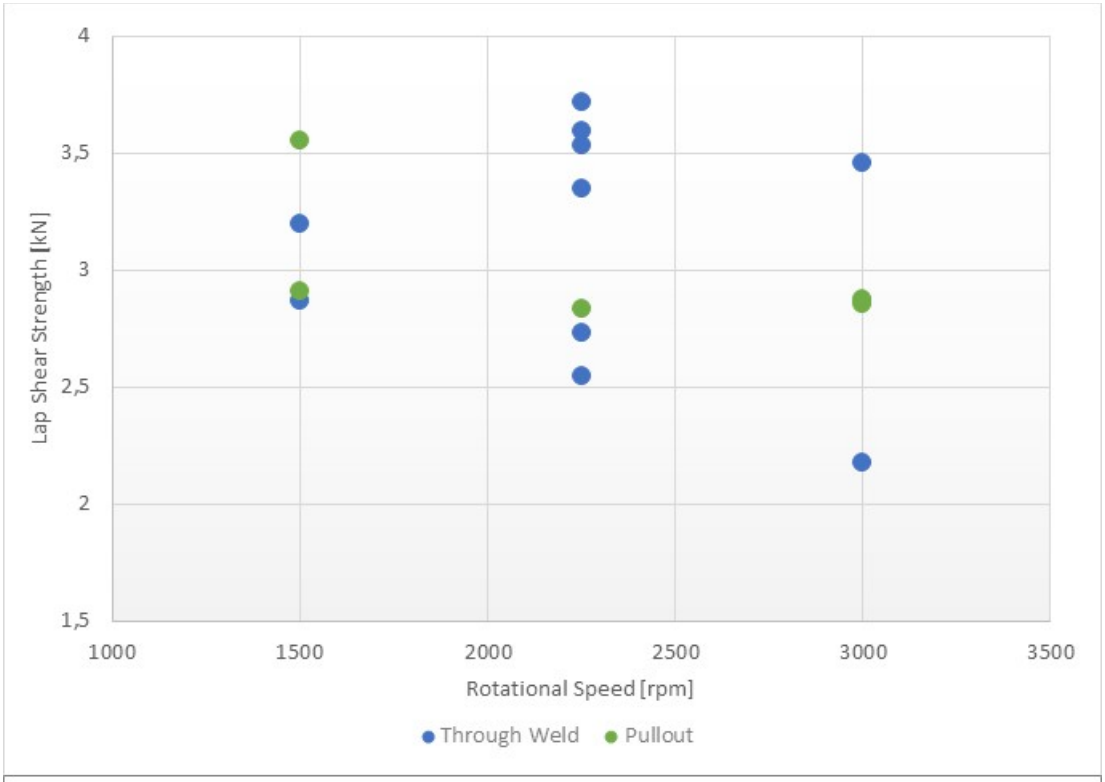
4
3,5
3
2,5
2
1,5
Lap Shear Strength [kN]
1000
1500
2000
2500
3000
3500
Rotational Speed [rpm]
Through Weld
Pullout

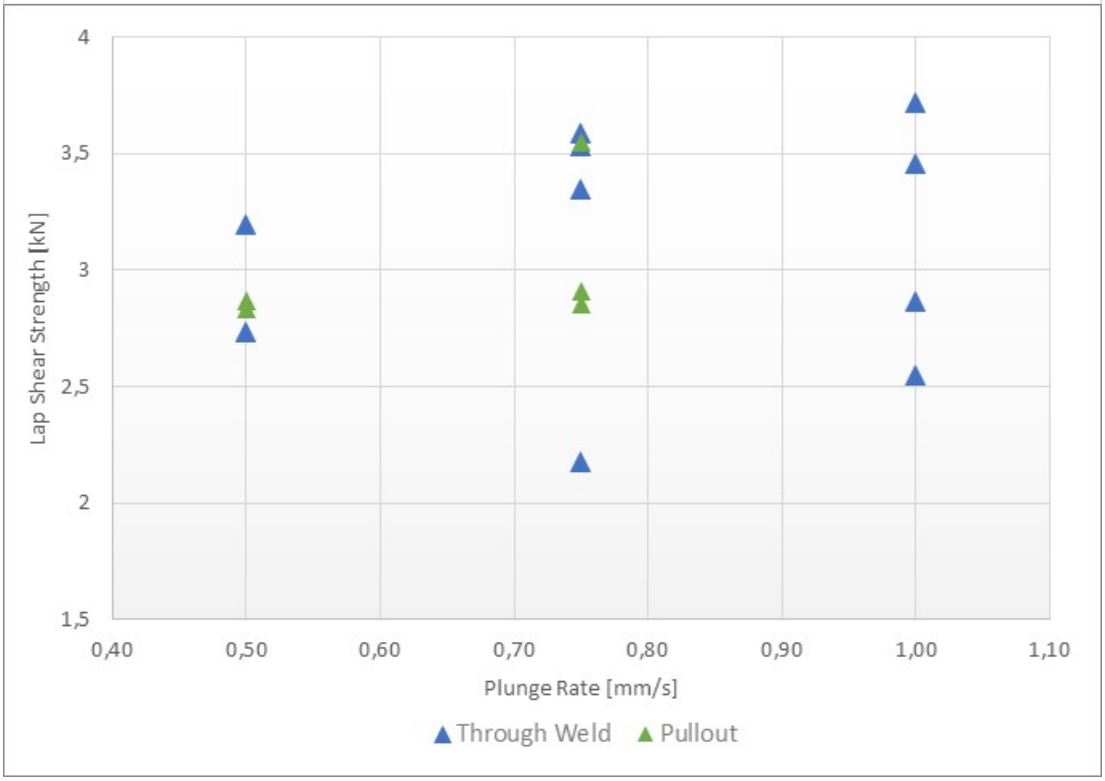
4
3,5
3
2,5
2
1,5
Lap Shear Strength [kN]
0,40
0,50
0,60
0,70
0,80
0,90
1,00
1,10
Plunge Rate [mm/s]
Through Weld
Pullout

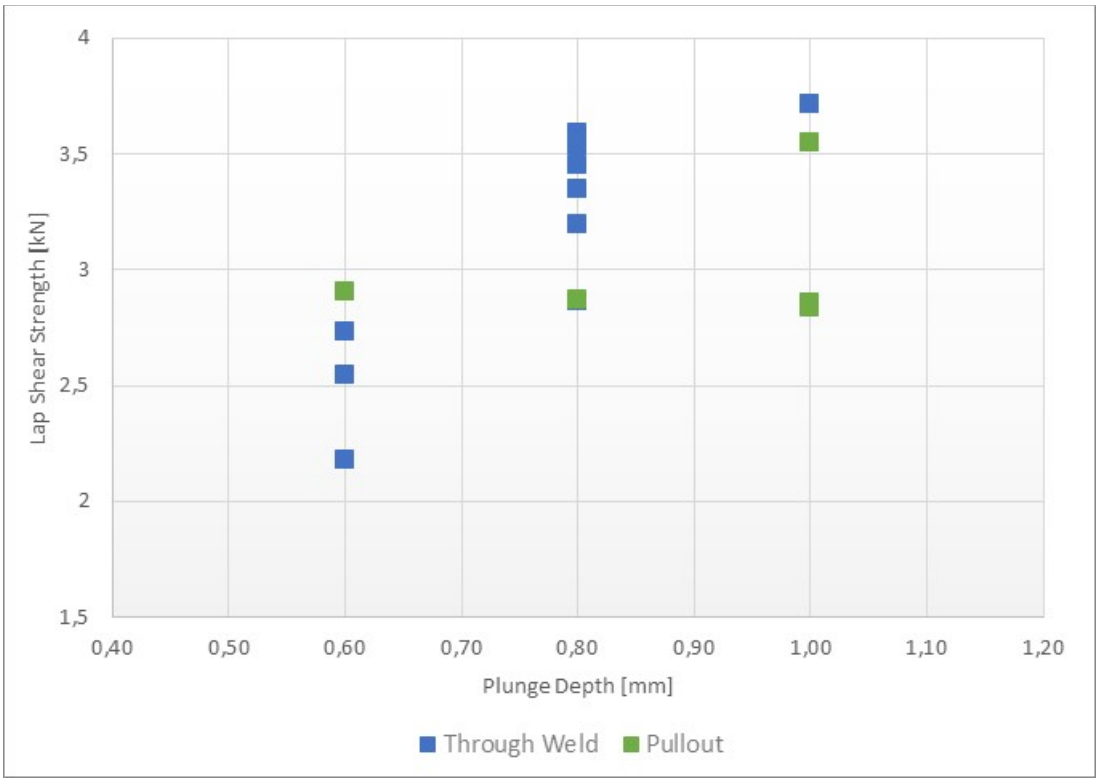

Figure 41 - Lap Shear Strength plotted against process parameters with different failure modes

Finally, the same type of plot was observed for Plunge Time in Figure 42, which is not a process parameter but varies as a function of Depth and Rate. Again, no apparent pattern is present, rendering any conclusion impossible to be drawn.

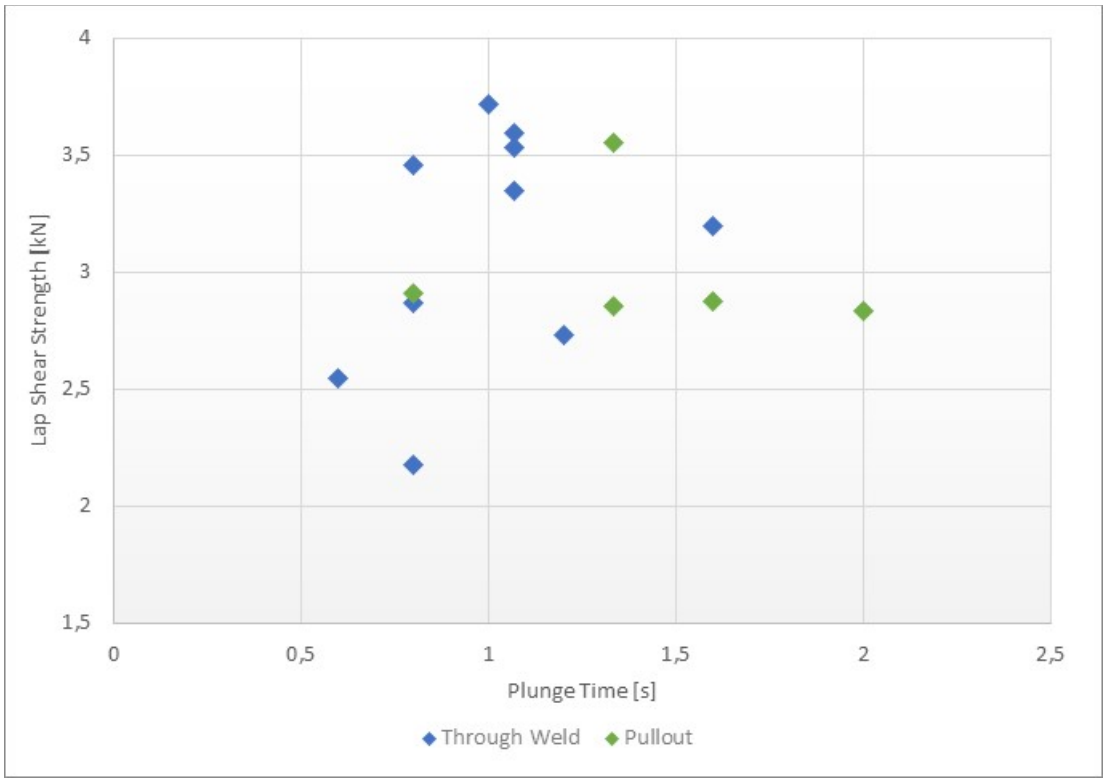

Figure 42 - Lap Shear Strength vs. Plunge Time with different failure modes.